Nanolines on silicon surfaces

A.B. McLean*

Department of Physics, Queen's University,
Kingston, ON, K7L 3N6, Canada
Fax: + 613 533 6463
E-mail: mclean@physics.queensu.ca
*Corresponding author

I.G. Hill

Department of Physics and Atmospheric Science,
Dalhousie University, Halifax,
N.S., B3H 3J5, Canada
E-mail: ian.hill@dal.ca

J.A. Lipton-Duffin and J.M. MacLeod

Department of Physics, Queen's University,
Kingston, ON, K7L 3N6, Canada
Fax: + 613 533 6463
E-mail: duffin@emt.inrs.ca E-mail: macleod@emt.inrs.ca

R.H. Miwa

Faculdade de Física, Universidade Federal de Uberlândia,
C.P. 593, 38400-902, Uberlândia, MG, Brazil
E-mail: hiroki@infis.ufu.br

G.P. Srivastava

School of Physics, University of Exeter,
Stocker Road, Exeter EX4 4QL, UK
E-mail: gps@excc.ex.ac.uk

Abstract: Although a wide range of periodic surface nets can be grown on low index silicon surfaces, only a few of these have quasi-one dimensional symmetry. If high index silicon surfaces, such as (553) and (557), are used instead, the surface unit cell contains steps. It is possible to fabricate a number of quasi-one dimensional nanoline systems on the terraces and some of these have nested energy bands near the Fermi level. These nano-scale systems may support exotic many-electron states produced by enhanced electron correlations and a reduction in electron screening in one spatial dimension. In this paper, our groups' experimental and theoretical studies of nanolines phases, grown on both low index and vicinal silicon surfaces are reviewed. These studies give us insight into the electronic properties of artificial nanoline structures.

Keywords: nanolines; one-dimensional physics; scanning tunnelling microscopy; electronic structure; highly correlated systems.

Reference to this paper should be made as follows: McLean, A.B., Hill, I.G., Lipton-Duffin, J.A., MacLeod, J.M., Miwa, R.H. and Srivastava, G.P. (2008) 'Nanolines on silicon surfaces', *Int. J. Nanotechnol.*, Vol. 5, Nos. 9/10/11/12, pp.1018–1057.

Biographical notes: A.B. McLean is a Professor of Physics at Queen's University, Canada. He obtained his PhD, *Microcontact Spectroscopy of magnetic metals*, at the University of Cambridge in 1985. His thesis supervisor was G.G. Lonzarich. He subsequently studied with Professor R.H. Williams, University College Cardiff, and F.J. Himpsel, I.B.M. Yorktown Heights, where he used angle-resolved photoemission with synchrotron sources to study electronic states located on semiconductor surfaces and at semiconductor heterojunctions. His research group at Queen's is currently using variable temperature scanning probes to perform local spectroscopy of nano-structures assembled from a few atoms/molecules.

I.G. Hill obtained his PhD at Queen's University in 1997 for his Dissertation, *Design of an Inverse Photoemission Spectrometer for Studies of Quantum Wires*. He then worked with Professor Antoine Kahn at Princeton University, studying the formation of organic semiconductor/metal and organic/organic interfaces. As a Member of the Technical Staff at the Sarnoff Corporation in Princeton, NJ, he worked on next generation flat-panel display technologies, large-area low-cost electronics, and robotic vision systems. He is currently an Associate Professor of Physics at Dalhousie University, Canada, where his research is focused on organic electronic materials and devices.

J.A. Lipton-Duffin completed his PhD in A.B. McLean's research group at Queen's University in 2006. His research program involved the study of the band-structure of quasi-one dimensional nanoline phases grown on stepped silicon surfaces with momentum-resolved inverse photoemission using an instrument that he built as a MSc student. These studies are described in Section 4.

J.M. MacLeod completed her PhD in A.B. McLean's research group at Queen's University in 2006. She used a home-built scanning tunnelling microscope to study bismuth nanolines grown on Si(001), the large scale modification introduced by the bismuth nanolines on the Si(001) step and terrace structure (Section 5), and atom clusters grown on the template afforded by the Si(111)-7×7 and the Si(111)-Ge(5×5) surface reconstructions. She is currently working as a postdoctoral fellow in F. Rosei's group at the Institut national de la recherche scientifique, Énergie, Matériaux et Télécommunications.

R.H. Miwa obtained his PhD, in July 1997 at the Universidade de Sao Paulo, Sao Paulo-Brazil. His supervisor was Professor A.C. Ferraz. He performed post-doctoral studies at the University of Exeter UK from July 1999 to July 2000, supervised by Professor G.P. Srivastava. Since June 2005 he has had a permanent position as an Associated Professor of Physics at the Instituto de Fisica, Universidade Federal de Uberlandia, Uberlandia-MG, Brazil. His research interests are theoretical/computational studies of solid materials, surfaces, interfaces, nanotubes and polymers, using ab initio and semi-empirical calculations.

G.P. Srivastava is a Professor of Theoretical Condensed Matter Physics in the School of Physics, University of Exeter, UK. He received from Banaras Hindu University, Varanasi, India, MSc in 1969, PhD in 1972, and DSc in 1980. His research interests include: theoretical investigations of group-state properties, electronic and phonon states in bulk semiconductors, surfaces, and nanostructures; ultra-fast non-equilibrium phonon dynamics; thermal conduction in bulk and nano-structured semiconductors. He has published more than 300 research papers, including ten review papers, and two postgraduate books: *The Physics of Phonons* (Adam Hilger, Bristol, 1990) and *Theoretical Modelling of Semiconductor Surfaces* (World Scientific, Singapore, 1999).

1 Introduction

The Si(001) and Si(111) surfaces are among two of the most extensively studied solid surfaces [1–3]. The Si(111) surface has a long-range surface reconstruction [3,4] that produces striking electron diffraction patterns. Unravelling the details of this complex reconstruction presented a significant challenge to surface science in the latter part of the 20th century [5–9]. Although fundamental studies of adsorption, diffusion, electronic structure, surface crystallography and growth are performed on both surfaces, Si(001) is the surface that is used to fabricate semiconductor devices.

In addition to the two-dimensional lattices, or surface nets, produced by the reconstruction of native silicon atoms on the Si(001) and Si(111) surfaces, a wide variety of adlayer systems, can be grown atop these surfaces by depositing metals from suitable sources in ultra-high vacuum [10,11]. Only a few adlayer systems can be grown with quasi-one-dimensional (quasi-1D) symmetry (Figure 1(a)) on flat silicon surfaces. Examples include Si(111)-In(4×1) [12–15], Si(111)-Au(5×2) [16] and the Si(111)-M(3×1) honeycomb chain-channel reconstruction where M can be one of the following monovalent metals: Li, Na, K, or Ag [17–19]. These systems all have three equivalent domains and each domain is related to the other two by simple rotation. To create a surface with a single domain, small vicinal offcuts, typically less than 5°, are used to create steps and stabilise one of the three domains at the expense of the other two [20,21]. The steps are present in relatively low concentration. They are not an integral part of the surface unit cell. Alternatively, by using a judicious choice of offcut angle, atomic steps can be integrated into the surface unit cell. Moreover, by depositing another atomic species onto these surfaces, it is possible to grow nanoline arrays that have rows of atoms embedded in the Si(111) terraces. This type of quasi-1D system is represented schematically in Figure 1(c).

Figure 1 A schematic representation of three different types of nanoline system that have been realised. (a) Parallel rows of adatoms on a metal (M) or semiconductor (S) substrate; (b) a stepped metal surface with adatoms decorating the edges of the terraces, producing a line or 'wire' [22] and (c) a stepped semiconductor surface with atoms embedded in the terraces producing, once again, a line or 'wire'. Reprinted with permission from [23]. Copyright 2006 by the American Physical Society

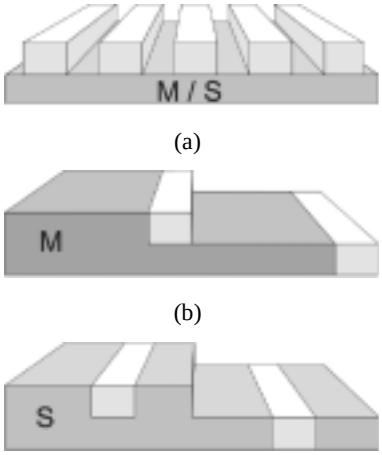

The three types of line phases, illustrated schematically in Figure 1, are examples of low dimensional systems produced by self-organisation that have been realised [2,24,25]. Valuable prototypes, they can be used to study the properties of electrons confined to weakly coupled line arrays with typical line widths of only 1 nm [26]. The single-electron properties of these systems, and in particular the relationship between electronic structure and geometry, is of interest. However, it is their many-electron properties that have attracted most attention [24,26]. It is widely expected that these quasi-1D systems will support exotic many-electron states [13,27], and that may include the formation of charge density waves (CDW) [28–32] or a quantum fluid with collective spin and charge fluctuations [33,34]. In 1D, the long-lived fermionic quasiparticles that are present in two and three spatial dimensions are unstable. Fermi-liquid theory, the 'standard model' of interacting electron systems, is replaced by alternate formalisms [33–35].

Because these line phases are grown on top of metallic or semiconducting surfaces, they are accessible to scanning tunnelling microscopy (STM) [14,36]. Silicon is a well-understood material, and, therefore, it is a particularly convenient substrate to use. Because it is a semiconductor, there are no bulk states in the fundamental energy gap. Consequently, if a structural phase transition in the overlayer occurs [37], the region around the Fermi level can be studied with spectroscopic techniques, such as photoemission, inverse photoemission and STM, without interference from the bulk bands in the substrate. This greatly simplifies the interpretation of the experimental data and makes the identification of gap openings in the surface band-structure much more straightforward.

In this paper, we review our research groups' studies of nanoline phases grown on three different silicon surfaces: Si(111), Si(557) and Si(001). This paper is not intended to be an exhaustive review of nanoline physics or even nanolines on silicon surfaces. Instead we have selected some research topics that provide an overview of the research

that we have performed on three different nanoline systems that can be grown on silicon surfaces. Two of these are quasi-one dimensional systems that exhibit metal to non-metal transitions upon cooling below room temperature. The other is presented as a contrasting nanoline system that is of interest because it possesses striking structural quality and also because we have demonstrated that the growth of the nanolines affects the mesoscopic structure of the surface.

2 Experimental details

The experiments presented in this paper were performed with instruments designed and constructed at Queen's University. A brief overview of their capabilities will be given and citations are provided to publications describing the instruments in detail.

The STM experiments were performed with a home-built beetle-type microscope [38,39], shown schematically in Figure 2. This microscope was designed and built in 1999. It has been used to study the nanoline phases on silicon, and the growth of few atom clusters on the template afforded by both the Si(111)(7×7) and the Si(111)-Ge(5×5) [40] surface reconstructions.

Figure 2 The beetle-type scanning tunnelling microscope showing: the lifting assembly/beetle manipulator, used to raise the beetle off the sample holder and also to guide thin control wires; the sample holder, and part of the stacked-plate damping stage

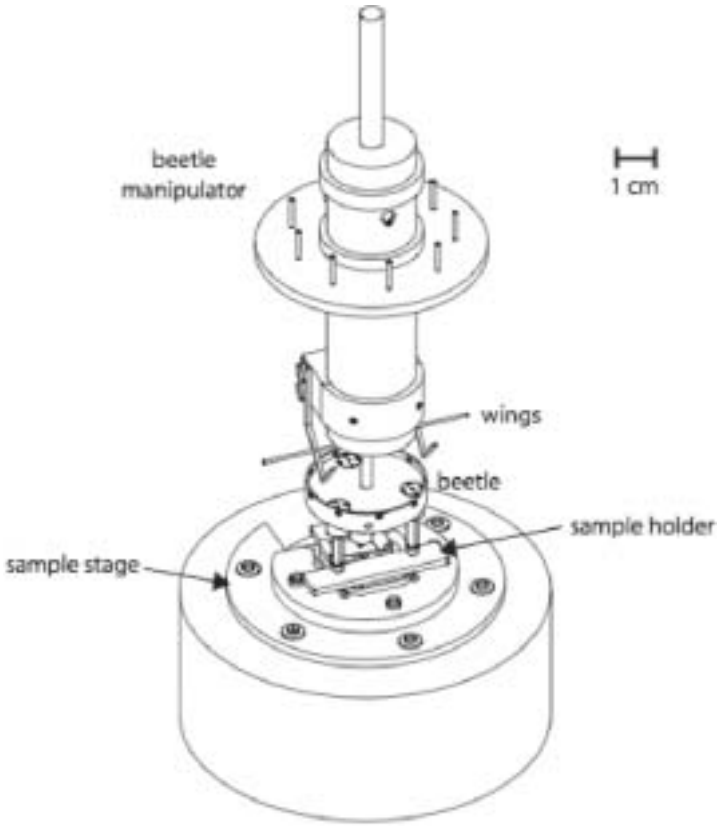

Light emission from the nanolines was measured using a home-built inverse photoemission system, comprising a Stoffel-Johnson low energy electron source [41] and two ethanol-filled Geiger-Müller photon detectors [42–44]. The photon detectors operate in isochromat mode. Photons with only one energy are detected, and the kinetic energy of the electrons is varied in such a way that final states, located between the Fermi level and the vacuum level, are probed. Both photon detectors are run at the same time. The detection energy is (10.78 ± 0.01) eV and the detectors have a (full width at half-maximum) bandwidth of (0.37 ± 0.02) eV.

Figure 3 (a) The Stoffel-Johnson electron source; (b) two photon detectors and (c) the sample and sample holder. The photon detectors make an angle of 50° with the high symmetry axis of the source. They are both mounted on linear drives and they can be pushed past the electron source without touching it, to increase the solid angle of detection. The drift tube mounted on the exit lens helps to create a field free region between the source and sample. Reprinted with permission from [23]. Copyright 2006 by the American Physical Society

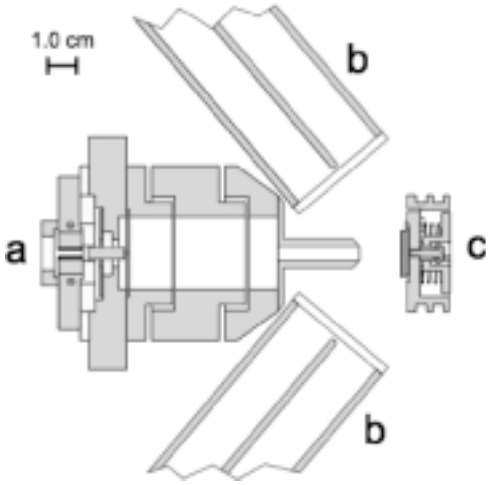

3 The S(111)-In(4×1) nanoline phase

Indium forms a three-domain (4×1) nanoline phase on Si(111) surfaces [12,14,21, 45–50]. The phase was prepared by adsorbing one monolayer (ML) of indium [51] onto the Si(111) surface. During deposition, the sample was held at a temperature of approximately 420°C, by resistive heating with alternating current. Following the deposition, this temperature was maintained for 5 min to promote the formation of large domains. The silicon surface had an intentional offcut that rotated the surface normal 3° towards the $[\bar{1}\bar{1}2]$ direction. This offcut produced terraces and steps. The steps run parallel to $[\bar{1}10]$. As mentioned above, the steps break symmetry and stabilise the (4×1) domain that has nanolines parallel to $[\bar{1}10]$. Low-energy electron diffraction was used to confirm the presence of a single (4×1) domain [49].

Figure 4 (a) A structural model of the quasi-1D Si(111)-In(4×1) system [50]. Indium atoms are rendered as black circles and silicon atoms are rendered as light grey circles. The dashed line is the oblique (4×1) unit cell. The centre-to-centre spacing of the indium nanolines is 13.3 Å and (b) one quarter of the Brillouin zone is shown with the commonly used symmetry labels. Reprinted with permission from [52]. Copyright 2000 by Elsevier Ltd

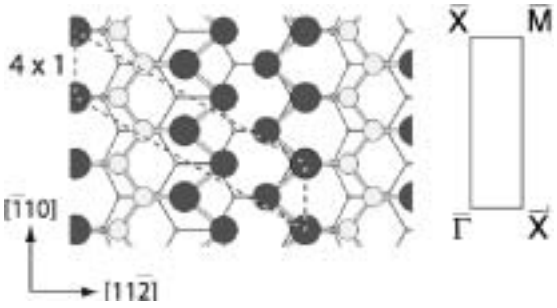

(a) (b)

This quasi-1D system (Figure 4) has attracted interest because it possesses a reversible metal to non-metal transition from a high temperature (4×1) to a low temperature phase, with lower translational symmetry, at approximately 115 K [13,53]. The translational symmetry of the low temperature phase has been designated ($4 \times$ '2') because both X-ray [54] and electron diffraction [13,53] patterns have half-order streaks rather than $2\times$ spots. This notation distinguishes it from a fully ordered system and indicates that there is a relatively small coherence length associated with the $2\times$ ordering. An early experimental study of this low temperature broken symmetry state postulated that the structural phase transition could be due to the formation of a quasi-1D CDW [53] or Peierls instability [55,56]. Electrons and holes in the vicinity of the Fermi level can couple strongly to a lattice vibration and produce a periodic charge modulation accompanied by a CDW energy gap at the Fermi level [53]. Although common in organic semiconductors, transition metal trichalcogenides and transition metal bronzes, charge density waves had not previously been detected in quasi-1D overlayer systems. This exciting suggestion was supported by the fact that near perfect Fermi-surface nesting was discovered with angle-resolved photoemission at room temperature [53]. This formation of the CDW has been vigorously debated in the literature.

For example, it has been shown, using X-ray diffraction, that even at 20 K the system does not condense into an ordered superstructure [54]. Although the earlier study [53] found half-order diffraction streaks at 100 K, it was expected that at lower temperatures the CDW would lock, due to finite interactions between the indium rows, into an (8×2) pattern, and this would be the *true* low temperature ground state. It was also noted, using high-resolution electron-energy loss spectroscopy, that there is a drastic reduction in the surface free carrier density when the system is cooled through the phase transition [57]. Despite this, the low temperature phase was not found to show complete semiconducting character at 90 K, a temperature that lies below the transition temperature. Moreover, subsequent theoretical calculations [58,59] did not support the simple CDW interpretation. Instead they supported the view that there was a number of structural ground states, or configurations, that were essentially degenerate. Above the transition temperature the average atomic positions would produce a (4×1) pattern due to dynamic

fluctuations [59]. The conclusions of the theoretical studies found support from a detailed X-ray diffraction study of the low temperature phase [54], where it was found that the (8×2) reconstruction possesses a high degree of (4×2) subcell disorder, or uncorrelated arrangements of both subcells along the indium rows.

This low dimensional system has a surprisingly complex band structure. For example, ab initio calculations predict that three bands should cross the Fermi level along the ΓX direction of the surface zone [58,60]. These bands are nested [53] and one of the bands crosses the Fermi surface at a wavevector that is approximately half way between Γ and X. Consequently, a charge density wave coupled to a lattice vibration, with a wavelength equal to two times the fundamental repeat period along the indium atom row, could produce a Peierls-like instability [55]. As mentioned above, the nature of the broken symmetry in this system, at low temperature, is still being actively studied (e.g., see [59,61–63]). Recent experimental work has focused on the study of the domain structure, or intertwined structural phases [63], as the system is cooled through the transition temperature with STM [61,63]. This has provided a direct picture of the fluctuation and condensation phenomena through the phase transition [61]. In the remainder of this section we will describe our studies of the unoccupied electronic structure of this system.

Although not surprising that the energy bands near the Fermi level have quasi-1D symmetry [13,53], it is remarkable that the energy bands at higher energies, that are more spatially delocalised, also reflect the quasi-1D symmetry. For example, the Si(111)-In(4×1) system possesses an image state resonance [47,49,52,64]. The state is spatially located in the near surface region, above the lines, and energetically located just below the vacuum level. We studied the band dispersion of this state and found evidence for anisotropic dispersion and a small energy gap in the image state band in the direction that is perpendicular to the nanolines [47]. Later we will return to discuss the formation of this resonant state.

In Figure 5, we reproduce the experimental band structure measured using inverse photoemission in the energy region located between the Fermi level and the vacuum level. Spectra were collected at incidence angles from –45° to +45° in steps of 5° along $[\bar{1}10]$, the direction parallel (||) to the nanolines. The second derivative of each spectrum was calculated to locate regions of high curvature (the bands), and then mapped onto a $(E, k_{||})$ grid. This allows the experimental energy bands to be visualised directly, and Figure 5 represents the experimental band structure measured along the ΓX direction of the surface zone. Of particular note are the Fermi level crossings (A) at $k_{||} = \pm 0.6$ Å^{-1} (see discussion above) and the image state resonance (B).

Along the ΓX direction (Figure 6), the dispersion of the image state is parabolic with an effective mass close to the free-electron value. However, perpendicular to the indium nanolines (ΓX′), the image state resonance is found to fall below the free electron parabola. The most straightforward explanation for this is that the electrons 'feel' the surface corrugation potential produced by the rows of indium atoms. The size of the lower Fourier components of the corrugation potential was inferred from the band dispersion in the perpendicular direction [47]:

$$V(x) = 1.07 \sin G_3 x + 0.41 \cos G_4 x,$$

where $G_n = n2\acute{}/a$, $a = 13.3$ Å and the coefficients, 1.07 and 0.41, are in units of V.

Figure 5 The experimental band structure of the quasi-1D Si(111)-In(4×1) system, in an energy range that spans both the Fermi and the vacuum level, measured using inverse photoemission along the ΓX direction of the surface zone The two features labelled A are Fermi level crossings. The feature labelled B is an image state resonance

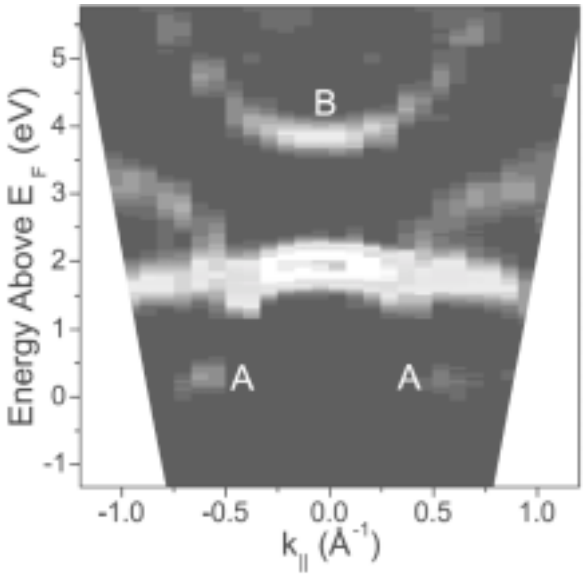

Figure 6 The measured dispersion of the image state resonance, both parallel (||) and perpendicular (⊥) to the indium nanolines, is illustrated using black circles. The solid line is a free electron parabola matched to the experimental points at the Γ point ($k_{||} = 0$). Note that in the perpendicular direction, the experimental points start to deviate from the free electron parabola at $\approx \pi/(13.3\ \text{Å}) = 0.24\ \text{Å}^{-1}$. This is the zone boundary of the 4×1 superlattice in the 4× direction. Reproduced with permission from [52]. Copyright 2000 by Elsevier Ltd

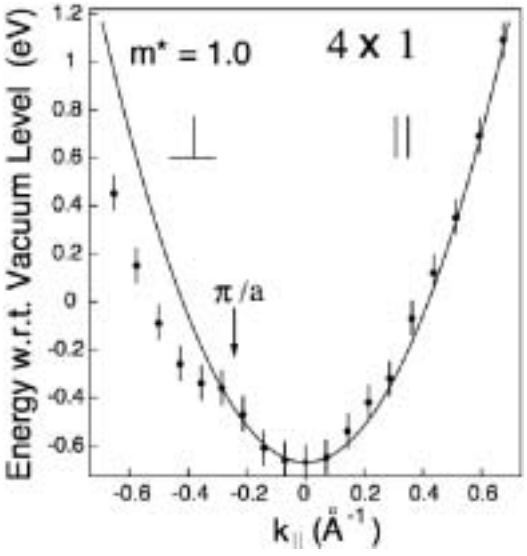

Theoretical investigations of the geometry, electronic states and image states in the Si(111)-In(4×1) system have been performed [60,65]. Here we will briefly describe the results obtained by Miwa and Srivastava [60]. The supercell implementation of the pseudopotential method was employed, within the density functional scheme [66], for the study of atomic geometry. A perturbative scheme [67] was used to calculate the energy dispersion of the most tightly bound image state.

The calculated width (Figure 7) of the indium nanoline was found to be 6.70 Å, and this is in agreement with the experimental observation that the separation between two neighbouring lines is å13.3 Å [50]. The two zig-zag rows of indium chains that comprise the line (Figure 7) are separated by 4.56 Å. Both zig-zag rows are buckled by 0.31 Å, with the edge atoms lying higher. The indium-silicon bond lengths are in the range 2.64–2.66 Å, close to the sum of the covalent radii of indium and silicon. The nearest neighbour distances in the indium chains are in the range 2.89–3.09 Å. The calculated geometry is in good agreement with X-ray diffraction measurements [50]. The calculated indium-indium distance lies in the range 2.89–3.09 Å. This is slightly shorter than the bulk indium value because there is a mixture of metallic and covalent bonding. Figure 7 contains a plot of both the theoretically determined atomic geometry and the total charge density.

Figure 7 (a) The theoretically determined atomic geometry of the Si(111)-In(4×1) reconstructed surface. The atomic distances are in Å and (b) the total electronic charge density is shown in units of 10^{-2} electrons per (a.u.)^3. Reproduced with permission from [60]. Copyright 2001 by Elsevier Ltd

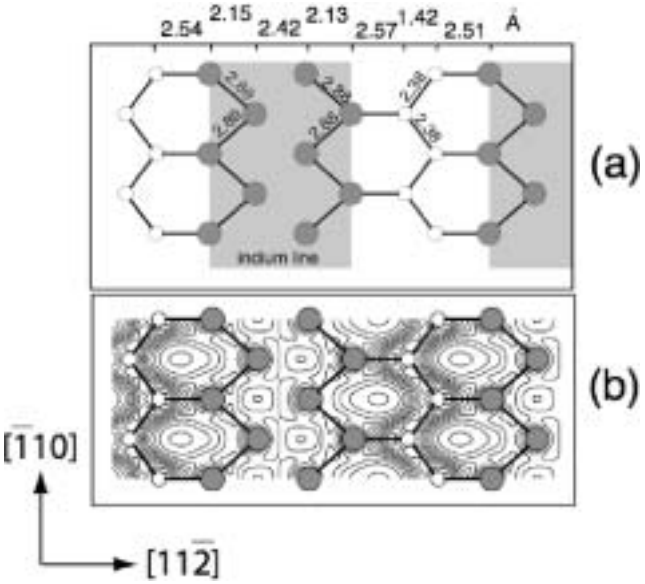

The electronic structure, calculated within the local density approximation, along the two principal symmetry directions on the surface Brillouin zone is shown in Figure 8.

Figure 8 Si(111)-In(4 × 1); calculated electronic structure. The shaded region is the silicon bulk continuum. Reproduced with permission from [60]. Copyright 2001 by Elsevier Ltd

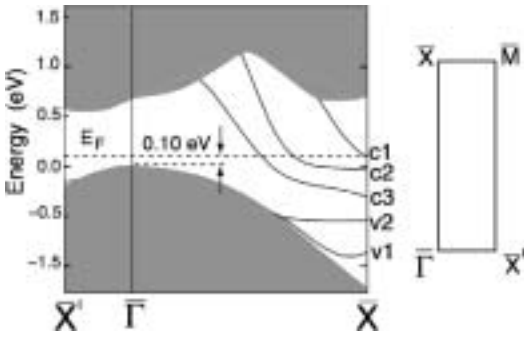

There are no surface states inside the silicon fundamental band gap along ΓX′, the normal to the indium chain direction. Along ΓX, the indium chain direction, there are up to five surface states within the silicon band gap region (v1, v2, c1–c3). The bands v1 and v2 are fully occupied, and the bands c1, c2 and c3 are partially occupied. The Fermi level lies at 0.1 eV above the silicon bulk valence band maximum. Along ΓX, the states c1, c2 and c3 show downward dispersion, crossing the Fermi level at 0.98ΓX, 0.69ΓX and 0.55ΓX, respectively. The Fermi level crossing agrees with experimentally obtained data [21,46]. Calculations suggest that the two partially filled bands, c2 and c3, are formed by localised sp bonding orbitals and p_z antibonding orbitals along the indium line, providing clear evidence for the quasi-1D nature of the system. The electronic distribution of surface states, v2, c3 and c2, are depicted in Figure 9.

Figure 9 Partial electronic charge density near to the X point for the: (a) v2 band; (b) c3 band and (c) c2 band. Units of 10^{-3} electrons per (a.u.)^3. Reproduced with permission from [60]. Copyright 2001 by Elsevier Ltd

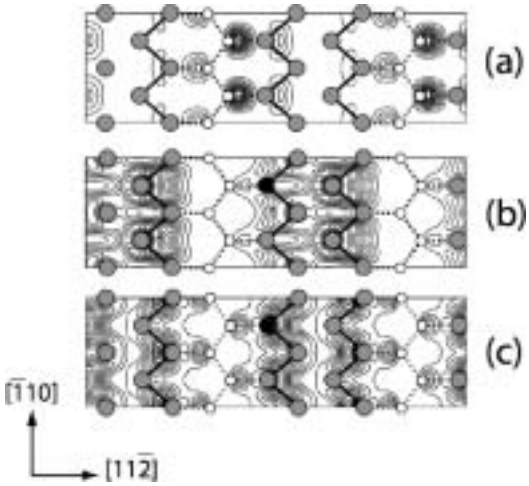

For calculating image state energies, the potential obtained within the local density approximation was modified to take the following asymptotic behaviour [67],

$$V(z) = -\frac{1}{2(z - z_0)}[1 - e^{-\lambda(z - z_0)}]; \quad z > z_0$$

in Ry units, where z_0 is the position of the image plane and λ is the inverse distance over which the image potential saturates. The image plane (i.e., z_0) was located at one-half atomic spacing beyond the last atomic layer in the slab and determined λ by matching $V_{IP}(z)$ with $V_{LDA}(z)$ at $z = z_0$. With this, we constructed $V_{IP}(z) = [(\varepsilon - 1)/(\varepsilon + 1)]V(z)$, with $\varepsilon = 11.9$ as the static dielectric constant of silicon. Image state energies were obtained by applying the first-order correction to the surface eigenvalues $E(k_{\|})$ obtained within the local density approximation

$$\Delta E(k_{\|}) = \frac{\langle \Psi_{LDA}(k_{\|}) | (V_{IP} - V_{LDA}) | \Psi_{LDA}(k_{\|}) \rangle}{\langle \Psi_{LDA}(k_{\|}) | \Psi_{LDA}(k_{\|}) \rangle}$$

where Ψ_{LDA} is the wavefunction within the local density approximation.

The dispersion of the most tightly bound $n = 1$ image state is presented in Figure 10. In agreement with our inverse photoemission measurements [47], the calculations predict a strong anisotropy of the image state dispersion. Along ΓX, parallel to the line, the effective mass of the image electron is close to the unperturbed free-electron value. However, along ΓX′, normal to the line, the dispersion does not follow a free electron parabola. The dispersion in the latter case can be explained using the nearly free electron model, assuming that there is an energy gap of approx. 0.1 eV at the X′ zone edge. The gap is associated with the surface corrugation potential normal to the lines. Calculations suggest that while there is a negligible surface corrugation potential along the indium line, there is a large surface corrugation potential normal to the line, as is shown in Figure 11. Therefore, there is an appreciable amount of asymmetry in the corrugation potential, with the deepest minimum being located at the more electronegative of surface species, *viz.* silicon atoms.

Figure 10 Si(111)-In(4 × 1); the calculated energy-dispersion relation for the most tightly bound $n = 1$ image state (a) along the indium lines and (b) normal to the indium lines. The theoretical results are represented using white circles and a parabola has been fit to the theoretical results. In addition, the experimental image state band structure is represented using black circles. The lines indicate the estimated energy and momentum resolution. The energy resolution reproduced here is smaller that that quoted in an earlier paper [47]. It represents a more recent and precise determination of the experimental uncertainty in the experiment. Reproduced, with permission, from [60]. Copyright 2001 by Elsevier Ltd

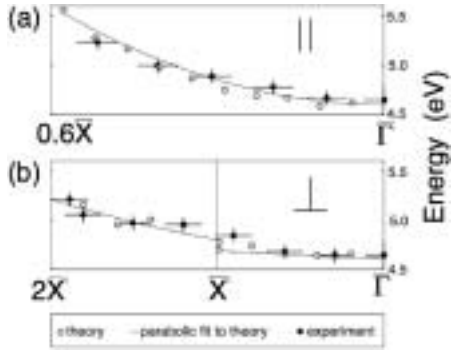

Figure 11 Partial surface corrugation potential for the Si(111)-In(4×1) system normal to the indium lines. Reproduced, with permission, from [60]. Copyright 2001 by Elsevier Ltd

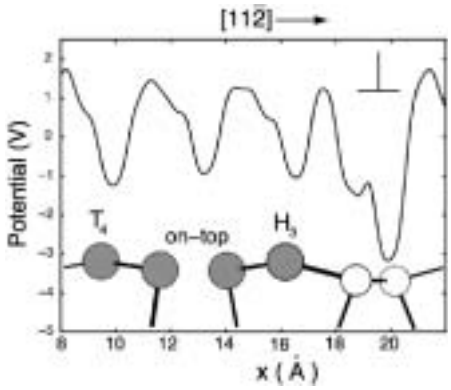

4 The Si(557)-Au nanoline phase

As mentioned above, adsorbing atoms on stepped silicon surfaces, created by a vicinal offcut, creates a variety of nanoline phases (Figure 1(c)) [27,68–70]. The advantages of using a stepped surface are that the width of the terraces and the spacing between the adatom rows can be changed. A shallower offcut corresponds to a larger terrace width. Moreover, by judicious choice of the offcut angle [27,69], the atomic steps become an integral part of the surface reconstruction and all the terraces have the same width [71].

The Si(557)-Au system (Figure 12) contains one row of gold atoms embedded in each silicon terrace. The rows are parallel to the steps that terminate the terraces and the gold inter-row spacing is equal to the silicon terrace width of 1.9 nm. At this spacing, the coupling between the rows of gold atoms is weak, and the two-dimensional system effectively becomes a one-dimensional system. However, by using a vicinal surface with a steeper offcut relative to (111), the terrace width can be decreased and the inter-row coupling can be increased. For example, on Si(553), the terrace width is 1.5 nm and, using angle-resolved photoemission, the increased coupling can be detected in the energy bands near the Fermi level [69]. Consequently, the coupling between the adatom rows that comprise the quasi-1D structure can, to some extent, be tailored.

A constant-current topographical STM image collected from the Si(557)-Au system is presented in Figure 13. The image area is 45×45 nm and the sample bias (+1.87 V) was chosen to probe empty states. Several features are striking. The steps, like the bismuth nanolines that will be described later, are very straight and devoid of kinks. In comparison, low index surfaces of silicon usually show a high number of kinks. Additionally, the terrace width is constant, leading to a very regular step structure. The silicon atoms at the edge of the step are thought to arrange themselves into a graphene-like layer [69,72], a configuration that is known to be particularly stable. The lattice matching along the terrace ($[1\bar{1}0]$) is excellent. This layer essentially lies above a silicon (111) lattice plane.

Figure 12 Top (a) and side (b) views of a structural model for Si(557)-Au [69]. The solid lines in panel (a) define the unit cell [70]. The full black circles represent silicon adatoms and the full grey circles represent gold atoms. Reprinted with permission from [23]. Copyright 2006 by the American Physical Society

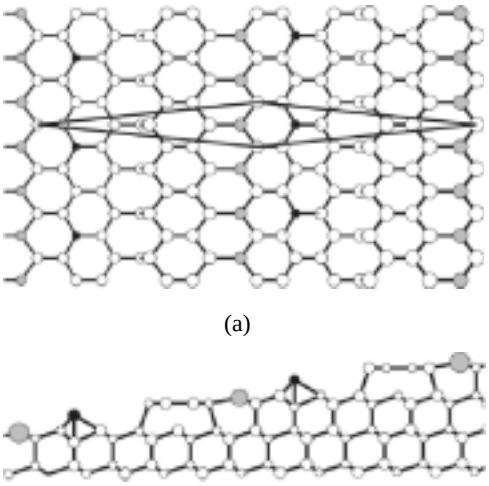

(a)

(b)

Figure 13 (a) An STM image of the Si(557)-Au system. The image area is 45×45 nm^2 and the sample bias was +1.87 V (empty states). The silicon adatoms that form rows with a $2\times$ periodicity are clearly visible, as are the streaks that are thought to arise from the silicon atoms located at the terrace edge and (b) a higher magnification image of the same surface, taken with a sample bias of +2.00 V, showing the silicon 2×1 adatom rows, the extra silicon adatoms and the short terraces that are inclined at 9.5°. The image area is 25×25 nm^2. Reprinted, with permission, from [23]. Copyright 2006 by the American Physical Society

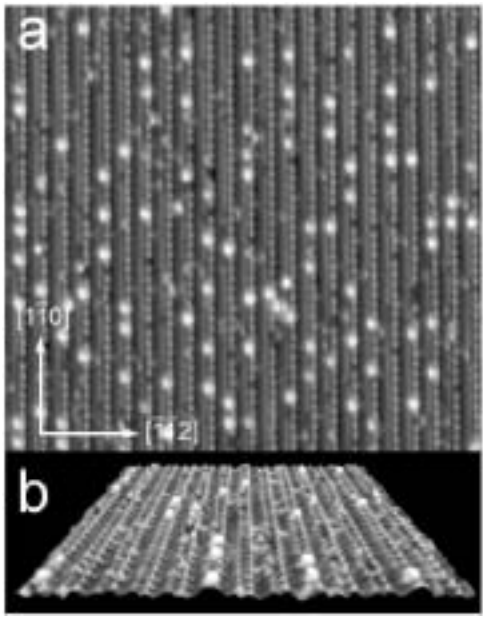

In Figure 13, the silicon adatoms that form rows with a 2× translational symmetry are clearly visible, as are the streaks that are thought to arise from the silicon atoms located at the terrace edge. In addition to these features, there is a low background concentration of 'extra' Si adatoms [69,73], which appear as bright spots in Figure 13(a). On the related Si(111)-Au(5×2) surface reconstruction, these extra adatoms show a preference for 4× ordering along the line [73]. The addition of one silicon adatom every four unit cells in Si(111)-Au(5×2) alters the electron count within the surface unit cell leading to a metallic surface. On Si(557)-Au we found that, along the adatom rows, even numbered extra adatom spacings are common and that the extra adatoms do not come closer than four surface lattice constants from each other. For example, we have not observed extra adatoms two or three surface lattice constants apart. In Figure 14(b) a linescan has been reproduced that clearly shows extra adatoms spaced by 4×.

Figure 14 (a) An STM image of Si(557)-Au. The image area is approx. 45×40 nm^2 and the sample bias was +2.00 V (empty states). The bright features are 'extra' silicon adatoms and (b) a linescan that clearly shows the 2× spacing, generated by the ordered rows of silicon adatoms, and two extra silicon adatoms that have a spacing of 4×. Several extra adatoms in this image have this spacing. See, for example, the row directly above the row that is marked

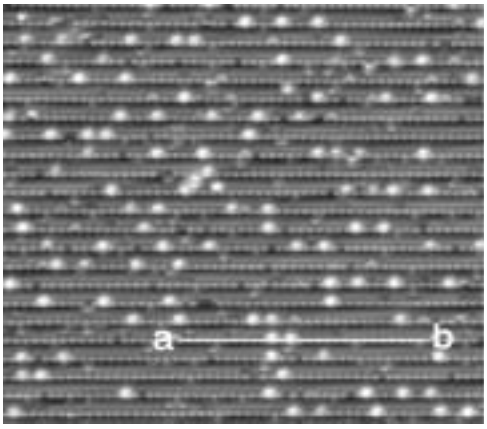

(a)

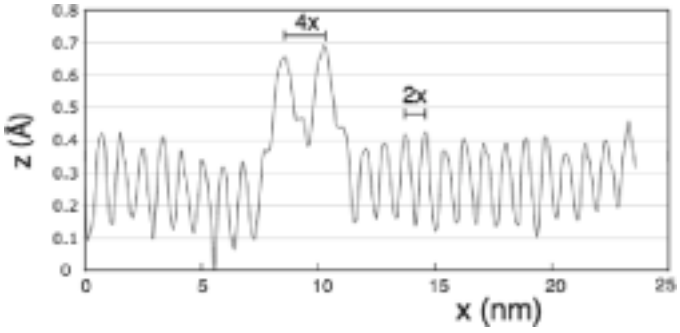

(b)

Interestingly, as with Si(111)-In(4×1), studies of the Si-Au quasi-1D overlayer systems have found multiple energy bands near the Fermi level, giving rise to nested sheets at the Fermi surface [69]. Some of these bands are metallic at room temperature and undergo metal to non-metal transitions [74] when the system is cooled below room temperature [68,69,75]. Athough the view is not universally held [76], it is thought that the metal to non-metal transitions in these systems are Peierls instabilities. Moreover, as mentioned above, it is expected that electron correlations in these quasi-1D systems with fractionally filled bands will give rise to exotic quantum fluids such as the Luttinger liquid [27,33,34,74]. Indeed, early studies of the Si(557)-Au system provided evidence for the absence of fermionic quasiparticles and the separation of spin and charge into collective spin and charge fluctuations [13,27]. This exciting possibility was later ruled out for Si(557)-Au by a more detailed angle-resolved photoemission study of the energy bands that exploited the tuneable nature of synchrotron radiation to maximise the photoemission cross-section [77]. Although the features that were interpreted as spinon and holon bands had different group velocities, they did not intersect at the Fermi level.

In fact, the physical origin of the bands near the Fermi level has still to be satisfactorily established. The two partially occupied bands (designated S1 and S2 in [75]) just below the Fermi level in the Si(557)-Au system both have a parabolic dispersion and resemble the spin-orbit split surface states found in the neck of the bulk Fermi surface near the L point on Au(111) [78]. The role of relativistic corrections to the band structure in the Si(557)-Au system has been investigated with ab initio theoretical approaches [76], and it was demonstrated that the spin-orbit interaction does generate two bands that have a similar dispersion over a large part of the surface zone. However, recent temperature dependent experimental studies [75] performed with STM and angle-resolved photoemission demonstrated that S1 and S2 behave quite differently. The experiments found that the S2 band was gapped at room temperature whereas S1 was metallic. Upon cooling, a gap was also observed to open in the metallic S1 band. The metallic S1 band has been associated with silicon atoms at the terrace edge that undergo a Peierls-like periodic lattice distortion [55]. In this scenario, the electronic phase transition is localised to the terrace edges.

In Figure 15, the experimental band structure of the Si(557)-Au system, measured with inverse photoemission, is presented. Feature A is a band, or a closely spaced doublet, that disperses down towards the Fermi level and then crosses at $k_{\|} = (0.5 \pm 0.1)$ Å^{-1}. This is in excellent agreement with previous photoemission studies [75,79]. The earliest of these two studies [79] found two closely spaced bands (S1 and S2, mentioned above) which crossed the Fermi level at $k_{\|} = 0.38$ Å^{-1} and 0.44 Å^{-1} respectively. The latter study [75] found the Fermi level crossing to occur at $k_{\|} = 0.35$ Å^{-1} and 0.41 Å^{-1}. The two bands have a splitting of only 0.3–0.4 eV. Consequently, the individual bands can not be resolved with inverse photemission because the total energy resolution (electrons and photons) is $\Delta E \approx 0.42$ eV. Despite the fact that the two bands merge into one single feature, the good agreement between the location of the Fermi level crossing obtained from both photoemission and inverse photoemission has the obvious explanation that they are the same feature.

Figure 15 The experimental energy bands, of the Si(557)-Au system measured with inverse photoemission, along the ΓK and the ΓM′Γ symmetry directions. The Fermi level is taken as the zero of energy. The bands clearly illustrate the quasi-1D nature of the surface electronic structure; there is weaker dispersion perpendicular to the atom rows (ΓM′Γ) than there is along the rows (ΓK). The fact that feature A disperses down towards the Fermi level suggests that the system is a band-metal

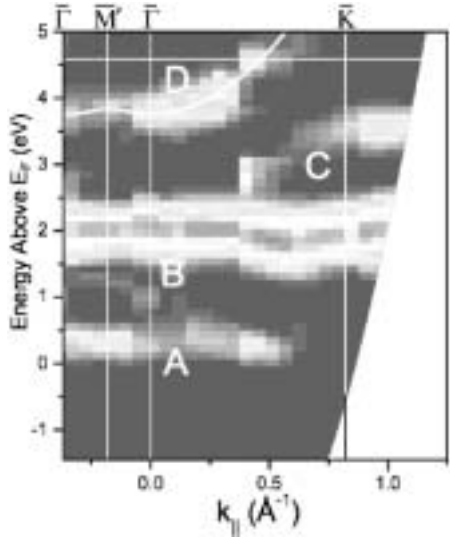

There is also a state, labelled D, located just below the vacuum level that resembles the image state resonance found on Si(111)-In(4×1) nanoline system. The width of state D (not shown) is significantly larger than the width of the Si(111)-In(4×1) image state resonance. State D also has parabolic dispersion parallel to the nanolines. This is the expected behaviour for free electron-like image state band. In the perpendicular direction, the dispersion of feature D is quite flat, indicative of spatial localisation and quasi-1D symmetry.

It is plausible that the physical origin of the two states lying just below the vacuum level in Si(557)-Au and Si(111)-In(4×1) is similar. It is unlikely that the states are conventional image states [80] because there is no bandgap in the substrate band structure in this energy range. Consequently, the crystal potential will not Bragg scatter electrons into the surface region. This suggests that, at most, the states are image state resonances, and similar to the resonant state found on Al(111) [81–83]. The large state linewidth, found for Si(557)-Au, supports this conclusion. The overlap with the bulk continuum could lead to a reduction in the lifetime of the state. In fact, the state could be incipient. However, the physical factors that stabilise image state resonances in nanoline phases are not well understood. Presumably the surface potential generated by the overlayer plays an important role in localising the state within the near surface region, as it does on Al(111) [84,85]. But it is unknown why the width of the image state on Si(111)-In(4×1) is smaller that the width of the image state on Si(557)-Au. More theoretical and experimental studies are required to understand the electronic structure of these systems and studies of the image state lifetime with two-photon photoemission [86–88] would be informative.

5 Nanolines on Si(001)

The nanoline phases share several physical attributes: they all contain parallel and regularly spaced lines; they are all grown on the Si(111) surface or a vicinal surface, created by cutting a silicon crystal close to (111). We will now describe the bismuth nanoline system [89] that is grown on Si(001) ([90] and refs. therein), the device growth surface. In some respects, it is similar to Si(111)-In(4×1) and Si(557)-Au, but in other respects it is an interesting contrast. A constant-current topographical image of ten irregularly spaced nanolines, grown on Si(001), is reproduced in Figure 16. Interestingly, although the silicon terraces between the lines contain a large number of vacancies and a depletion hole, the structural quality of the lines is very high. Although defects in the lines are occasionally observed (e.g., see the sixth line from the left in Figure 16), we have never observed a kink in the bismuth lines. These findings are in good agreement with previous studies [89–100].

Figure 16 Ten bismuth nanolines grown on a Si(001) surface. The bias voltage used to collect the image was $V_{sample} = -2.47$ V (full states) and the image size is 47×47 nm^2. Between the bismuth lines there are: silicon dimer vacancies, lines of silicon dimer vacancies running parallel to the bismuth lines and a depletion hole (top left) with a depth of two silicon layers. Reprinted, with permission, from [101]. Copyright 2004 by the American Physical Society

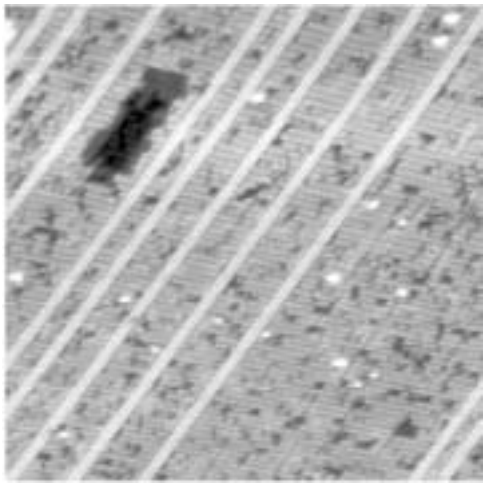

At first glance, the structural integrity of the lines appears to suggest a process where the bismuth lines nucleate and then grow in a ‘chain’ reaction. Although we do not intend to suggest that the bismuth lines form in the same way, molecular lines can be fabricated on hydrogen terminated Si(001), using a radical chain reaction [102]. Furthermore the molecular lines form without extensively reconstructing the silicon substrate. The surface acts as a directing template for anisotropic growth of the line [103,104]. If an unpaired silicon dangling bond is created with the STM tip, and subsequently the surface is exposed to styrene vapour, a surface benzyl radical forms. This is stabilised by H abstraction from the neighbouring Si-H site [105] and regenerates the dangling bond in the silicon surface. This assembly process leads to molecular lines. The growth of molecular lines occurs along the silicon dimer rows because the lattice spacing (3.84 Å)

matches the size of the adsorbed styrene molecule. Interestingly, the bismuth lines grow preferentially across the silicon dimer rows. Although the assembly of the bismuth lines can not be directed with the STM tip, the quality of the bismuth lines is superior to that of any organic nanoline grown on Si(001). Under optimal growth conditions, the length of the bismuth lines appears to be limited only by the availability of free space on the silicon terraces. The size of the available silicon terraces does not ultimately restrict the growth of the lines: the lines can modify the silicon surface to increase the areal size of silicon terraces. Although the line width is only 1.5 nm, the line length can be as large as 500 nm. Therefore, the lines introduce long-range correlations into the surface structure.

The main motivation for studying these line structures is to understand the physical mechanisms that lead to the high structural quality. The bismuth lines do not have exotic electronic properties; they are conventional semiconductors. Because they have a low density of states around the Fermi level, they also make very poor electrical conductors. For this reason, they are sometimes called quantum antiwires [106,107]. To put the bismuth nanoline system in a broader context, one of the primary goals of nanoscience is to control the composition and structure of materials, devices and sensors at the atomic/molecular level. In recent years, the focus has moved from layer-resolved growth, used in molecular beam epitaxy, to the control of composition in all three spatial directions and at length scales down to one nanometer. This leads to great control of material properties. However, new methodologies must be found in order to assemble large numbers of nano-structured systems on a practical timescale [108]. One way of achieving this goal is to utilise systems that can be assembled in parallel. For systems assembled on surfaces, different terms in the surface free energy can be used to guide the assembly process [109,110]. On semiconductor surfaces, morphological instabilities that arise from either anisotropic strain fields [111], or growth kinetics [110], can be used to break symmetry and create dots [112], huts [113,114] or wires [25,115,116]. However, it is very rare to find structural elements that have the quality of the bismuth nanolines. For this reason, the structural and electronic properties of the lines have been studied in detail.

The bismuth lines shown in Figure 16 were grown on n-type Si(001) wafers that had resistivities in the range 5.2–7.2 Ωcm and misorientation angles $|\theta| < 0.5°$ The Si(001) surfaces were prepared by resistively heating the silicon samples to 1260°C for 40 s while maintaining the chamber pressure below 2×10^{-9} Torr, annealing at 1000°C for 180 s, and then slowly cooling the sample at a rate of 1°C/s. The sample temperature was measured using an infrared pyrometer. Bismuth line arrays were then grown on these surfaces by depositing 0.5–4.5 ML of bismuth at a rate of approx. 0.07 ML/min in the desorption regime ($T > 500$°C), the temperature range where bismuth has enough thermal energy to escape from the Si(001) surface into the vacuum. The samples were subsequently annealed for 10–40 min at the same temperature.

At high biases, the bismuth lines are also very easy to image with STM. In agreement with other experimental studies [89,95,96,99], we find (Figure 17) the lines to be considerably 'brighter' than the surrounding silicon terraces in constant-current topographical images, when the applied bias lies above |1.5| V. In this voltage range, the lines really stand out from the silicon terrace. In principle, this phenomenon could arise from the presence of an energy gap within the line. However, our ab initio calculations indicate that the size of the energy gap within the line is much smaller than ≈3 eV. To try and understand the physical origin of the line/terrace contrast in STM images, we performed calculations of the tunnelling current using the Tersoff-Hamann

scheme [117,118]. These are described below. First, we describe the two structural models of the line that have the lowest calculated total energy.

Figure 17 Sequentially acquired images in the same region showing the bias dependence of the apparent height of bismuth lines. The image area is 300×300 Å^2; sample biases are: (a) –2.25 V; (b) –2.00 V; (c) –1.75 V and (d) –1.50 V. The arrowed lines in the images indicate the location for the line profiles presented beneath the images. The profiles clearly show a decrease in apparent line height with decreasing bias voltage magnitude. Reproduced with permission from [118]. Copyright 2005 by the Institute of Physics

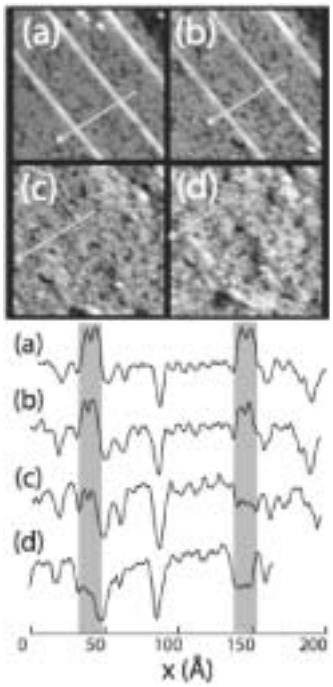

The theoretical calculations were performed in the framework of the density functional theory, within the local density approximation (LDA) using the Ceperley-Alder correlation [119], as parameterised by Perdew and Zunger [120]. The electron-ion interaction was treated by using norm-conserving, ab initio, fully separable pseudopotentials [121,122]. The wave functions were expanded in a plane wave basis up to the kinetic energy cutoff of 12 Ry. This energy cutoff was adequate for our studies: the total energy and the equilibrium atomic geometry were well converged to within 0.1 eV/(2×8) cell and ± 0.02 Å, respectively. To simulate the Bi-covered Si(001) surface we used a repeated slab method, with a supercell containing ten atomic layers of silicon and a vacuum region equivalent to twice the cubic lattice constant. We modelled the system by considering a unit cell with (2×8) periodicity. In order to test convergence of results we also made calculations with a (2×12) surface unit cell. The silicon dangling bonds on the other side of the slab were saturated using a layer of hydrogen atoms. The sampling of the surface Brillouin zone was performed using a set of four special k points. A dipole correction method [123,124] was employed to annul the effect of the spurious electrostatic field that arises due to the in-equivalence of the two surfaces in the

periodic slab geometry. To obtain the equilibrium geometry, atoms in the eight topmost layers were fully relaxed to within a force convergence criterion of 12 meV/Å.

Figure 18(a) is the Miki model of the bismuth nanoline; there are two parallel rows of bismuth dimers oriented along the [110] crystallographic direction. The separation between the two bismuth dimer rows in the Miki model is 6.62 Å. Normally there would be a row of silicon dimers on the surface in the region between the two rows of bismuth dimers. This row is missing. The Haiku model [100], shown in Figure 18(b), is also built from symmetric bismuth dimers, a stable entity on Si(001) due to the fact that bismuth has a valence of five. However, the distance between the bismuth dimers (6.32 Å) is 0.29 Å smaller than the distance calculated for the Miki model. The Haiku model also has missing silicon dimer rows and the silicon substrate below the line is reconstructed, forming three fivefold and two sevenfold rings. There are other important differences between these two models. For example, in the Miki model, the bismuth dimers (ignoring the lateral shift produced by the missing silicon dimer row) are in the positions that we would expect to be occupied by the silicon dimers. However, in the Haiku model, the bismuth dimers are shifted laterally by approximately $a_o/2$. Another way of thinking about this difference is to use the mirror plane of the bismuth line. In the Miki geometry, the mirror plane passes through the position a silicon dimer would occupy. For the Haiku geometry, the mirror plane is located between the silicon dimer positions. Consequently, it is possible to distinguish between these two line geometries by measuring the location of the line with respect to the lattice created by the silicon dimers. We will return to this later.

Figure 18 The two line models that have the lowest total energy: (a) the Miki ad dimer model has two parallel bismuth dimers separated by a missing dimer line. The line occupies three surface unit cells ($3a_o$) and (b) the Haiku model involves significantly more reconstruction of the surface and subsurface layers. In both (a) and (b) a vertical dotted line has been added to indicate the position of the mirror plane for the two lines

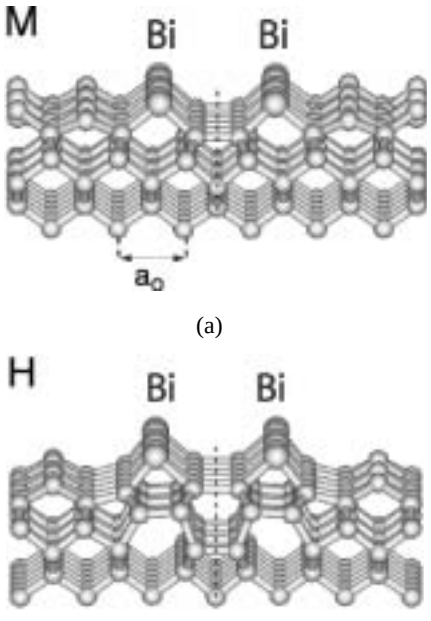

In order to determine the most stable atomic configuration, we compared the total energies of these two models by using the following expression:

$$\Delta E = E[H] - (E[M] + 2\mu_{Si}).$$

Here $E[H]$ and $E[M]$ represent the calculated total energies of the Haiku and Miki models, and μ_{Si} is the chemical potential of bulk silicon. To ensure that the same criterion was used for total energy convergence, the chemical potential of bulk silicon was calculated using the procedure we adopted for the surface (bismuth line) calculations. In agreement with other calculations [100], we found that the Haiku model was more stable than the Miki model by 0.37 eV/bismuth dimer. The convergence of our calculated ΔE has been verified with respect to:

- energy cut-off for the plane wave expansion
- number of special k point for the Brillouin zone sampling
- size of the surface unit cell.

In Figure 19(a) and (b) we present the calculated density of states (DOS) in and around the silicon bulk fundamental band gap for the Miki and the Haiku models, respectively. The DOS was calculated by considering the four special k points used for the Brillouin zone sampling. In both diagrams, the zero energy was chosen to be coincident with the highest occupied v1 peak. In the energy range –1 eV to +2 eV, there is a great deal of similarity in the DOS for the two models, except v4 shifts to a slightly lower energy for the Haiku model.

Figure 19 Calculated density of states for the bismuth lines on Si(001): (a) the Miki (M) model and (b) the Haiku (H) model. The valence band states v1–v4 are labelled on the figure and referred to in the text. Reproduced with permission from [118]. Copyright 2005 by the Institute of Physics

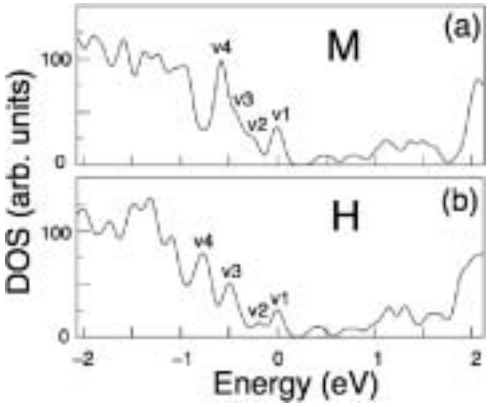

The silicon dimers located on the terraces between the bismuth lines buckle, producing both an ‘up’ and a ‘down’ atom within the silicon dimer. For the Miki model (Figure 20), our calculations reveal that the main contribution to the v1 peak results from the up atom on the terraces between the lines. The contribution from the bismuth dimers is a factor of ten smaller. Similar electronic distribution has been verified for v2. At ≈0.4 eV below v1, the v3 peak is formed with almost equal contributions from the π^* orbitals of the bismuth

dimers and the π orbitals from the silicon dimers. In contrast, for the v4 peak, lying at ≈0.58 eV below v1, the major contribution comes from the bismuth dimers.

Figure 20 Simulated constant current STM images of the occupied states, for the Miki model for three energy intervals within the valence band: (a) 0.2 eV; (b) 0.75 eV and (c) 1.7 eV. In (d) we present the vertical position of the 'tip' along the (solid and dashed) lines in the simulated constant-current topographical image. The vertical and horizontal positions are given in Å. Reproduced with permission from [118]. Copyright 2005 by the Institute of Physics

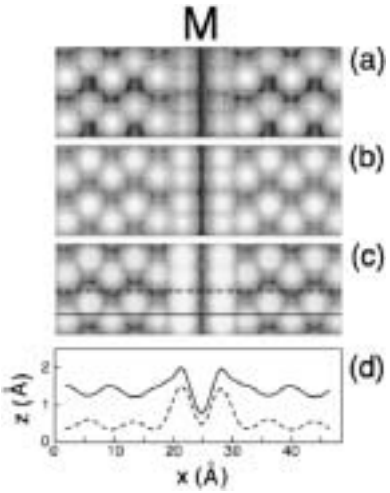

A similar scenario is found for the Haiku line geometry (Figure 21). The v1 and v2 peaks exhibit a very weak contribution from the bismuth dimers, being mainly concentrated along the silicon dimers. In contrast, the v3 peak, located 0.5 eV below v1, has almost equal electronic contributions from the π^* states of the p orbitals of the bismuth dimers, and the π states of the silicon dimers. The peak v4 lies at 0.78 eV below v1, with the main electronic contribution from the π bonding states localised along the bismuth dimers and also a contribution from the σ-like orbitals of the silicon dimers that is a factor of ten smaller. These results, for both structural models, are in accordance with the quantum antiwire property of the bismuth lines, namely:

- for low bias voltage, the STM image of the bismuth lines is darker than the silicon dimer plane for tunneling current from electronic states near the fundamental band gap
- with increased bias voltage, the bismuth lines become brighter than the silicon dimers.

Based upon our calculated electronic structure, we find that for low bias voltages, the tunnelling electrons come from the v1 and v2 peaks that are mainly localised on the silicon dimers. For increased voltages the electronic contribution from v3 and v4 peaks become dominant. The electronic states responsible for these features are mainly localised along the bismuth dimers, at ≈1 eV below the valence band maximum at v1.

Figure 21 Simulated constant current STM images of the occupied states, for the Haiku (H) model considering three energy intervals within the valence band: (a) 0.2 eV; (b) 0.75 eV and (c) 1.7 eV. In (d) we present the vertical position of the 'tip' along the (solid and dashed) lines in the simulated constant-current topographical image. The vertical (z) and the horizontal (x) positions are given in Å. Reproduced with permission from [118]. Copyright 2005 by the Institute of Physics

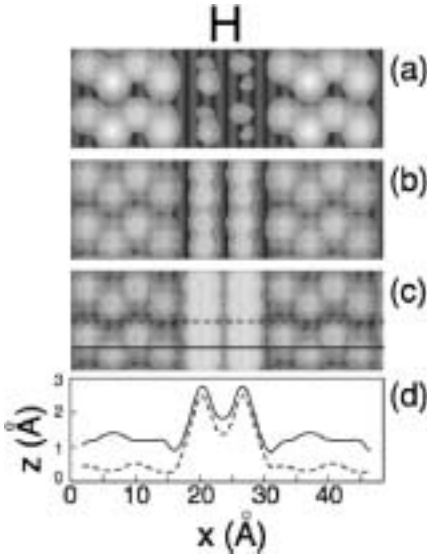

Another group has investigated the bias dependence of the STM images using density functional theory (DFT) for the Haiku model [99]. Rather than use the Tersoff-Hamann approximation [117,125], they calculated the projected charge densities associated with states within 0.2, 0.6 and 1.0 eV of the Fermi level. In agreement with our calculations, they found that the states near the Fermi level were located on the silicon terrace. Interestingly, they also demonstrated that the two silicon dimers that are located closest to the bismuth line (four in total; two on the left and two on the right) show a "greatly enhanced charge density in the states within 0.2 eV of the Fermi level". This was interpreted in terms of a line-induced strain field [99].

As aforementioned, we will now discuss the registry of the bismuth lines with respect to the silicon dimer lattice in the topmost silicon layer. In Figure 22, a linescan taken across a bismuth line (a) is reproduced together with the constant current topographical image (b) that was used to generate the linescan. A lower magnification image of the same area is provided in Figure 25. Figure 25 is dominated by two nanolines that run from the top to the bottom of the image. The line profile was taken from the line that is on the right hand side of the image (white dotted line). Care was taken to ensure that there were no bismuth dimers on the Si(001) terraces close to the bismuth line in the region where the line profile was taken. A portion of the line that was far from the ends was selected, the ends being outside the scan range.

Figure 22 (a) A linescan taken across a bismuth nanoline with a bias of V_{sample} = –2.09 V. The shaded region indicates the full width half maximum line width of å $3a_o$ and the dotted horizontal line is a baseline defined as the average of the line profiles on the silicon terraces adjacent to the line. A vertical dotted line indicates the approximate position of the mirror plane and (b) the image that was used to generate the linescan in panel (a). The mirror plane that passes through the centre of the line is coincident with the lattice created by the silicon dimers in the (001) surface. Reproduced with permission from [126]. Copyright 2005 by Elsevier Ltd

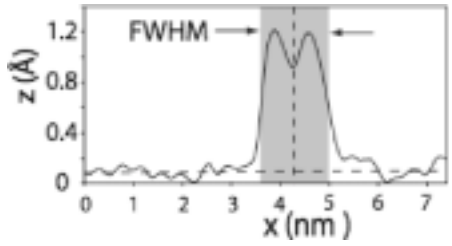

(a)

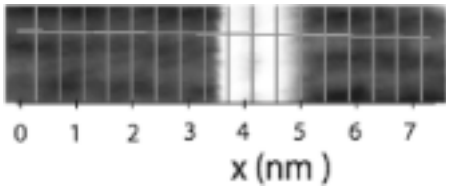

(b)

Added to Figure 22(b) are vertical lines coincident with the positions of the silicon dimers in the surface layer. The dotted horizontal line in Figure 22(a) is a baseline, defined to be the average height of the linescan on either side of the nanoline. It is assumed that the local maxima can be attributed to silicon dimers when the linescan is taken along the dimer rows. This figure demonstrates that our experimental line profile is 'in-registry' with the silicon dimer lattice. The mirror plane that bisects the bismuth line is coincident with the lattice created by the silicon dimers in the surface layer. Most published studies of line registry [93,97,100] have been performed on surfaces that were exposed to hydrogen after nanoline growth. Hydrogen passivation is used to ensure that the silicon atoms in the surface layer are clearly identified. However, our results are in conflict with the line profiles taken from surface exposed to hydrogen, where it was found that the lines were out-of-registry with the lattice created by the silicon dimers [100]. Our simulations suggest that hydrogen passivation should not complicate the determination of registry [118]. Consequently, an alternate explanation for this difference must be found. Fortunately, a simple explanation does exist.

In Figure 23 an STM constant-current linescan that intercepts a nanoline has been matched to the silicon dimer lattice in two different ways. In Figure 23(a), the silicon dimer lattice has been drawn coincident with the mirror plane that passes through the centre of the line. The mirror plane coincides with one of the silicon dimers in the Si(001) surface. In Figure 23(b), the silicon dimer lattice has been displaced, to the left, by half a surface lattice constant and compressed by 90%. The compression ensures that the positions of the dimers in the model match the local maxima associated with the silicon dimers in the linescan. From this comparison, it is clear that it is not straightforward to

distinguish between the in-registry (a) and the out-of-registry (b) line geometry using a linescan that samples only a few silicon dimers on either side of the nanoline. This is due, in part, to the fact that the nanoline occupies and therefore obscures part of the silicon dimer lattice. Consequently, it is natural to ask, can the two approaches be distinguished by sampling a larger portion of the silicon terrace?

Figure 23 An STM linescan, taken through a bismuth line, has been matched to the silicon dimer lattice in two different ways. In (a), the silicon dimer lattice has been drawn coincident with the mirror plane of the nanoline. A silicon dimer lattice, minus the bismuth line, has been reproduced below the linescan in top view. The scale of the model has been chosen so that the peaks in the linescan match the positions of the silicon dimers and in (b), the linescan has been shifted to the left by half a surface lattice constant and compressed in the horizontal direction by 90% to match the peaks in the linescan to the position of the dimers in the model (see the text)

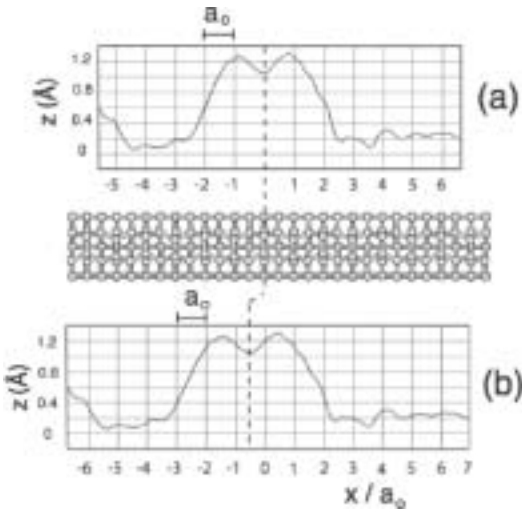

In Figure 24 a longer linescan has been reproduced. (The constant-current topographical image that the linescans of Figures 23 and 24 have been extracted from is reproduced as Figure 25.) This linescan traverses a distance equivalent to 34 lattice constants (from $x = -29$ to $x = +5$). It also perpendicularly bisects two bismuth lines, three ad-dimers (c, f and e) and a total of 20 silicon dimers.

Figure 24 A linescan that intercepts 20 silicon dimers in the silicon (001) surface plane, two bismuth nanolines and three ad-dimers (c, e and f). See the text for more details. $V_{sample} = -2.09$ V (full states)

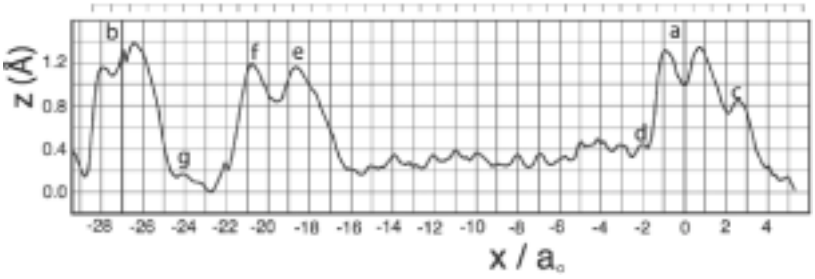

Figure 25 A low magnification version of the image that was used to generate the line profiles of the previous three figures. Specifically, the line profile presented in Figure 24 was from point a to point b and the line profile presented in Figure 22 was from point c to point d. The image size is 33×33 nm^2 and the bias voltage was $V_{sample} = -2.09$ V (full states)

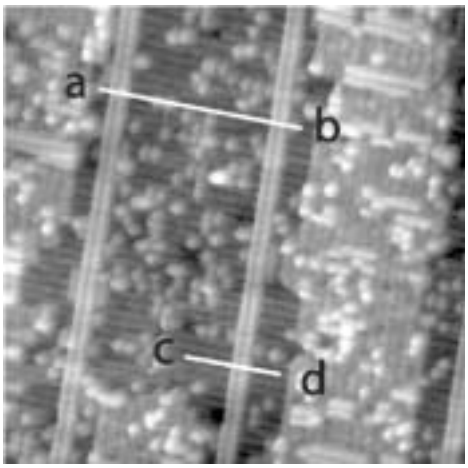

In-registry and out-of-registry silicon dimer lattices were matched to this linescan using the following two procedures. For the former, the dimer lattice was constrained to be coincident with the mirror plane of the line located to the right of the image (centred on $x = 0$). Then, the lattice was stretched to match the local maxima, produced by the silicon dimers on the (001) silicon surface, that are found at positions $x = -2, -3, -4$ etc. Because there are so many silicon dimers in the linescan, there is no ambiguity in this process. From the topographical image, it is known that the peaks labelled c, e and f are ad-dimers. In all cases, the peaks corresponding to the ad-dimers are out-of-registry with the silicon dimer lattice as expected; silicon has the diamond crystal structure. It is likely (Figure 25) that e and f are silicon dimers rotated by 90° with respect to the silicon dimers in the (001) terrace. The silicon dimer lattice is also found to be coincident with the mirror plane of the second line, located 27 lattice constants to the left of the first line ($x = -27$). This provides a check for self-consistency and additional support for the view that the bismuth lines are in-registry with the silicon dimer lattice. The linescan through the left line is slightly asymmetric. The asymmetry is produced by a bismuth dimer that has a voltage contrast that is different from the other bismuth dimers (Figure 25). This behaviour has been observed before [99] and it could indicate that there is an adsorbate such as hydrogen or water on the line. We have also reproduced an out-of-registry silicon dimer lattice in the upper portion of Figure 24 (grey lines). This lattice has been displaced by half a lattice constant to the left and then compressed by 90%, as before (Figure 23), to match the location of the three peaks on either side of the nanoline located at the origin. Overall, the out-of-registry lattice matches the peaks in the linescan very poorly away from the region where it is explicity matched to the linescan. The 90% compression of the silicon dimer lattice generates a surface lattice constant that is too small to provide a good description of the linescan over large distances. This illustrates the importance of using a long linescan to determine the registry of the line.

There is another feature in this linescan that deserves mention; at $x = -2$ there is a well-resolved local maximum. This feature is not resolved in all linescans. For example, in Figure 22 it merges with the intense feature located close to $x = -1$ thought to be a bismuth dimer. In Figure 23(a) there are shoulders on both sides of the line at positions $x = -2$ and $x = +2$, although neither are resolved as peaks. The feature at $x = -2$ is most likely a silicon dimer and its observation is significant because the Haiku model (see Figure 18) predicts that the first silicon dimer should be located at $x = 2.5$, two and a half lattice constants from the line centre. The experimental detection of a dimer at $x = 2.0$ is incompatible with Haiku. Moreover, Figure 25 also contains an ad-dimer at $x = 2.5$. Based on Haiku, we would expect the first ad-dimer to be located at $x = 3.0$.

What physical factors lead to line formation? First, we note that the line models with the lowest total energy are built from bismuth dimers. This is because the bismuth dimer is a stable entity on Si(001). Bismuth has a valence of five and, consequently, two bismuth atoms can form a dimer with two fully occupied lone pairs. Group V atoms break silicon dimers, fill silicon-dangling bonds and form symmetric bismuth dimers [127]. In contrast, silicon has a valence of four, and although the formation of dimers lowers the number of dangling bonds on the surface by two, it also leaves two dangling bonds. Because the dangling bonds are partially occupied a metallic surface state band results. It is well known that the metallic surface state band is unstable [3], and the silicon dimers buckle to open up a gap in the surface state band producing a semiconducting surface. Consequently, bismuth favours symmetric dimers whereas silicon favours asymmetric dimers. This is illustrated in Figure 26. Both symmetric bismuth dimers and asymmetric silicon dimers are important components of bismuth nanoline models (e.g., Figure 28).

Figure 26 (a) Schematic, side view, structural models of the Si(001)(2 × 1) surface with asymmetric Si-dimers and (b) the Si(001)-Bi(2 × 1) surface with symmetric Bi-dimers and calculated total charge densities. The white spheres represent silicon atoms and the black spheres represent bismuth atoms. Reproduced with permission from [128].

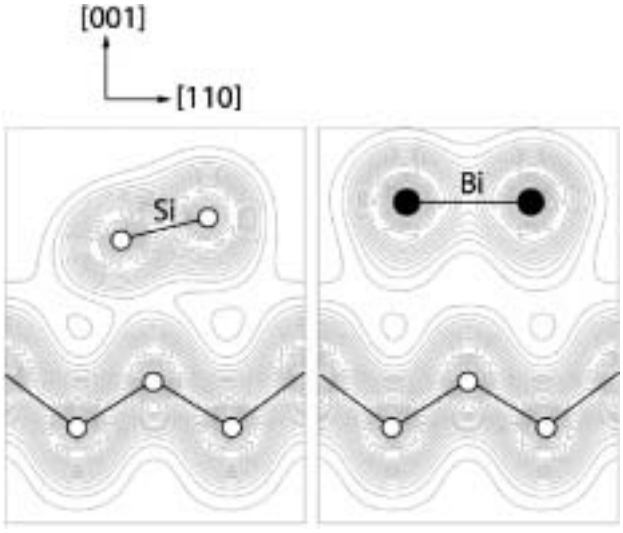

(a) (b)

Figure 27 A side view of a bismuth overlayer on Si(001). The 2× order is due to bismuth dimers and the *n*× order is due to missing Bi dimers. Reproduced with permission from [128]. Copyright 2005 by the Institute of Physics

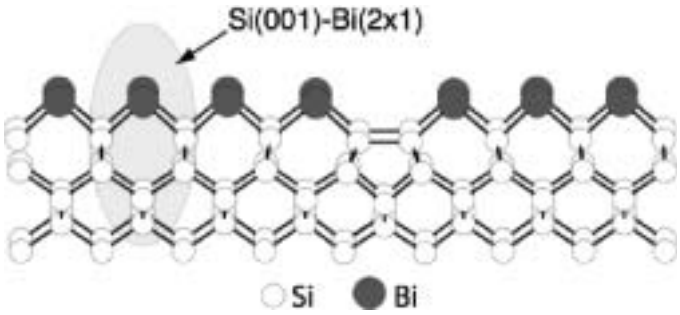

Figure 28 The influence of lines on the Si(001) step structure. (a) Bismuth deposition results in lines (L) inlets (I) and peninsulas (P). Approx. area; 500×500 nm^2. $V_{sample} = -1.85$ V. This surface was prepared by maintaining a temperature slightly above 590°C during the 10-minute deposition of approx. 1.4 ML of bismuth, and subsequently annealing for an additional 10 minutes at the same temperature. (b) For comparison, a clean Si(001) surface that was subject to a similar post anneal cycle shows a more even distribution of A- and B-type terraces, indicated by A and B in both figures. $V_{sample} = -2.00$ V. Approx. area; 1×1 μm^2. This surface was prepared by maintaining a temperature near 590°C for 40 min immediately following sample cleaning. Reprinted with permission from [101]. Copyright 2004 by the American Physical Society

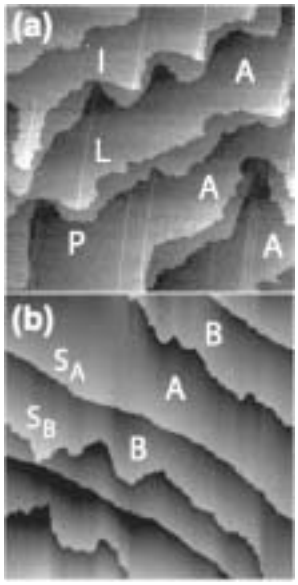

Second, it is known that the 25% mismatch in the covalent radii of bismuth and silicon (146 pm and 117 pm respectively) produces considerable strain. This is expected to play an important role in guiding the formation of the lines [100]. Clearly, one has to look no further that the Si(001)-Bi($2 \times$ n) surface reconstruction (Figure 27) that forms when bismuth is deposited on Si(001) at room temperature and then annealed below the line formation temperature. Park et al. [129] found that a series of well-ordered

$(2 \times n)$ superlattices, with the index n, ranging from 5 to 12, form. These superlattices are created by ordered rows of bismuth dimer vacancies that relax the compressive strain along the bismuth dimer rows [127,129]. Although the index n depends upon the annealing conditions, it does not drop below 5 [129]. This suggests that there is an elastic repulsive force between neighbouring missing bismuth rows. Furthermore, the formation of bismuth dimers on Si(001), produces an anisotropic surface stress. Surfaces, which reconstruct with broken orientation symmetry and have an anisotropic stress tensor are unstable to the formation of elastic stress domains and these can take the form of stripes [130]. Along the dimer bond the stress is tensile because the bonds to the silicon substrate prevent the bismuth atoms from coming as close as they would like [127]. As mentioned above, the stress perpendicular to the dimer bond (or parallel to the dimer rows) is compressive and the stress anisotropy produced by group *V* adsorbates, in a (2×1) surface net on Si(001), is known to increase linearly with increasing adsorbate atomic size [127]. Antimony, for example, also forms line structures, as long as 300 nm, on Si(001) [131,132].

Our experiments suggest that when the lines are produced by annealing bismuth-rich surfaces in the desorption regime, the Si(001)-Bi$(2 \times n)$ system plays an important role in guiding the formation of the nanoline arrays. However, the transition from the $2 \times n$ phase to the nanoline phase is complex and not fully understood. When the lines are formed by depositing sub monolayer amounts of bismuth onto a hot surface (550°C), the intermediary Si(001)-Bi$(2 \times n)$ adlayer reconstruction is bypassed, to a much greater degree, and line nucleation and growth appears to evolve differently [90,98,133]. A mechanism has recently been proposed to explain how the Haiku structure could be reached starting with bismuth ad-dimers [133].

Finally, we turn to describe the way that the bismuth lines modify the distribution of steps and terraces on the Si(001) surface. Because silicon has the diamond crystal structure, (001) surfaces separated by a single height step have the dimerisation direction rotated by 90° [1]. We adopt the standard convention that a type A step has the dimer rows parallel to the step edge and a type B step has the dimer rows perpendicular to the step edge. A type A terrace lies 'above' a type A step and a type B terrace lies above a type B step. Bismuth line growth is accompanied by a substantial amount of silicon mass transport. Rather than terminating at a step, the bismuth lines protrude on peninsulas that jut out from the silicon terrace. Recent STM studies performed above room temperature found that the peninsulas were not created by step erosion [90]. These peninsulas dominate the step edge structure on surfaces with a high areal concentration of lines. Likewise, lines also cut or plough into the terrace above, causing the silicon terrace to part, creating inlets. Indicative of silicon transport, islands of silicon and depletion holes, one or two layers deep, in the silicon terraces are also found. These surface features are now well documented in the literature [89,91–93,95–97].

We have also discovered that when bismuth lines are grown on Si(100) surfaces that have a regular distribution of single height steps, a single domain orientation is produced [101]. This preferential domain orientation is observed in samples that are prepared with high bismuth coverage and long and/or hot anneals. The STM image presented in Figure 29 contains a large domain that was produced using this approach.

Figure 29 A low magnification image of a Si(001) surface with an array of bismuth lines and a very large domain that extends over most of the image. The image size is $1.2 \times 1.2\ \mu m^2$ and the bias voltage was $V_{sample} = -2.5$ V. The growth of the bismuth line array creates a very flat surface, islands and depletion holes. However, the bismuth lines modify the terrace edges (top left) creating inlets and peninsulas. Reproduced with permission from [134]. Copyright 2005 by Elsevier Ltd

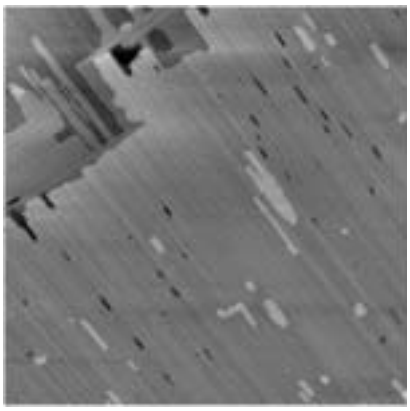

The surface shown in Figure 30 was prepared by depositing 2.3 ML of bismuth, over 30 min, on a surface that was maintained at a temperature of approximately 590°C. The surface was subsequently annealed for an additional 20 minutes at the same temperature after terminating the bismuth deposition. The image shows a surface that is almost completely covered in A-type terraces and the peninsulas and inlets associated with line growth on these terraces clearly dominate the large-scale surface structure. In contrast, the lines on the remaining B-type terraces appear to be geometrically inhibited or constrained by the competing growth of lines on the A-type terraces. These images can be compared with STM images taken from rare-earth silicide nanowires arrays on Si(001) surfaces (e.g., [116]). The silicide nanowire arrays also produce large-scale modifications of the Si(001) surface.

Figure 30 A Si(001) surface covered with bismuth nanolines illustrating the formation of a single domain orientation. Image details: $V_{sample} = -2.41$ V; approx. area $1.0 \times 1.0\ \mu m^2$. Reprinted with permission from [101]. Copyright 2004 by the American Physical Society

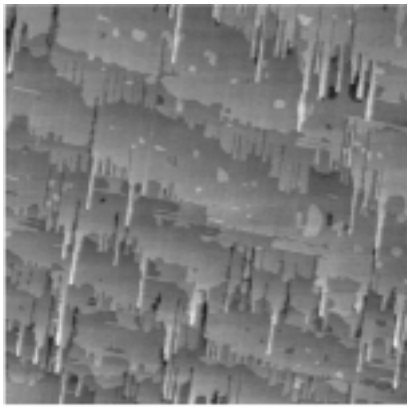

6 Discussion

We have described experimental and theoretical studies of three different nanoline systems, or phases, grown on three different faces of the silicon: Si(111), Si(557) and Si(001). The Si(111)-In(4×1) system is a conventional overlayer phase, set apart by its quasi-1D symmetry and the metal to non-metal transition that has been discovered in the quasi-1D surface bands. The system possesses multiple nested bands at the Fermi surface that suggest only weak coupling between the lines. The Si(557)-Au system is structurally more complex than Si(111)-In(4×1). It contains steps, embedded rows of gold atoms, silicon adatoms with 2× translational symmetry, a terrace edge structure that doubles its period at low temperature and extra silicon adatoms that form a regular superlattice. Significant progress has already been made in developing an understanding of this complex system. However, not all aspects of this system are understood. In particular, we described the electronic states located just below the vacuum level in both Si(111)-In(4×1) and Si(557)-Au. These may be analogues of the image states found on low index metal surfaces. Image states are not observed on Si(111)-7×7 and Si(557) surfaces with inverse photoemission. It is also not known why the image state linewidth on Si(557)-Au is so much greater than the corresponding state linewidth on Si(111)-In(4×1).

One general observation can be made about both systems. These two surface phases were singled out for study because it was widely expected that they would serve as useful prototypes of quasi-1D systems. It is probably fair to say that at the outset, few expected them to display such a panoply of physical properties. These ‘simple’ prototypes have not only provided significant challenges to our understanding but also, in many respects, exceeded our expectations.

The bismuth nanoline system, described above, represents an interesting contrast to both Si(111)-In(4×1) and Si(557)-Au. The bismuth lines form arrays. But the line spacing is irregular. The lines are also semiconductors. Despite the fact that they have a very interesting bias dependence in constant-current STM images, they do not belong to the growing class of (room temperature) metallic quasi-1D systems that can be grown on silicon surfaces. Nevertheless, the non-equilibrium growth conditions produce a line structure with striking structural quality that is only matched by the straight, kink free, step edges in the Si(557)-Au system. The physical factors that produce these straight lines are still being actively studied. The large (25%) mismatch between the covalent radius of bismuth (146 pm) and the covalent radius of silicon (117 pm) is expected to play a large role in guiding the formation of the lines [100]. Surprisingly, our STM studies have demonstrated that despite many years of concerted effort there are things that are still not fully understood about the equilibrium line geometry. STM line profiles, that we have collected, clearly show that the lines that we have grown are in-registry with the silicon dimer lattice. We have also collected STM line profiles that clearly show a dimer situated two surface lattice constants from the mirror plane of the line. One of these is reproduced in Figure 24. The accepted model of the line structure, the Haiku model [100], predicts that the first silicon dimer should be two and a half surface lattice constants for the line centre. We have also detected an ad-dimer two and a half lattice constants from the centre of a bismuth line. This is again, in conflict with the Haiku model. Based on Haiku, the first ad-dimer should be situated three lattice constants from the line centre.

Consequently, our STM results on three separate counts are in conflict with Haiku. These are:

- registry of the line with respect to the underlying silicon substrate
- detection of a silicon dimer two surface lattice constants from the line centre
- detection of an ad-dimer three surface lattice constants from the line centre.

Furthermore, our ab initio simulations have clearly shown that measurements of the line width are not sufficient to distinguish between the Haiku and Miki models. Does this mean that the Miki model provides a better description of the bismuth line? The Miki model is in registry with the silicon dimer lattice. Based on Miki we would also expect to find a silicon dimer two surface lattice constants from the line centre, and we would expect to find an ad-dimer two and a half surface lattice constants from the line centre. However, in our opinion, the most serious strike against the Miki model is the fact that it has a low kinking energy. To quote a recent review paper [90] "it was difficult to account for the extreme straightness of the nanoline with the Miki model, as the calculated kinking energy was very small, around 0.1 eV". We think it more likely that the correct line geometry still has to be found. The step-edge structures found at arsenic-terminated double-height steps on Ge(001) [135] provided an inspiration for the Haiku model. More recently is has been proposed that the 5-7-5 ring structure, that relieves strain at the arsenic-terminated step-edge, occurs in related systems such as As/Si(001) and P/Si(001) [136]. We have started to explore line structures that comprise two five-fold rings and one seven-fold ring. These line structures are more complex than the Miki structure but substantially simpler than Haiku. The latter comprises three five-fold and two seven-fold rings and penetrates five layers below the surface. We are optimistic that structures of this type will provide a good description of the bismuth nanoline.

Acknowledgements

Financial support was provided by the Natural Sciences and Engineering Research Council of Canada. We acknowledge discussions with Professor P. Dowben. Oliver Bunk kindly provided electronic source for Figure 4.

References

1 Zandvliet, H.J.W. (2000) 'Energetics of Si(001)', *Rev. Mod. Phys*., Vol. 72, No. 2, p.593–602.

2 Röttger, B., Hanbücken, M. and Neddermeyer, H. (2000) 'Nanostructure obtained by self-organization of silicon surfaces', *Appl. Surf. Sci*., Vols. 162–163, p.595–598.

3 Mönch, W. (1995) 'Semiconductor surfaces and interfaces', in Ertl, G. (Ed.): *Springer Series in Surface Science*, 2nd ed., Vol. 26, Berlin, Heidelberg, Springer-Verlag, New York.

4 Schlier, R.E. and Farnsworth, H.E. (1959) 'Structure and adsorption characteristics of clean surfaces of germanium and silicon', *J. Chem. Phys*., Vol. 30, No. 4, p.917–926.

5 Binnig, G. and Rohrer, H. (1986) 'Scanning tunneling microscopy', *IBM J. Res Dev.*, Vol. 30, No. 4, p.355–369.

6 Binnig, G. and Rohrer, H. (1982) 'Scanning tunneling microscopy', *Helv. Phys. Acta*., Vol. 55, p.726.

7 Binnig, G. and Rohrer, H. (1986) 'Scanning tunnelling microscopy – from birth to adolescence', *Rev. Mod. Phys*., Vol. 59, No. 3, p.615–625.

8 Binnig, G., Rohrer, H., Gerber, Ch. and Weibel, E. (1982) 'Surface studies by scanning tunneling microscopy', *Phys. Rev. Lett*., Vol. 49, p.57–60.

9 Takayanagi, K., Tanishiro, Y., Takahashi, S. and Takahashi, M. (1985) 'Structure analysis of Si(111)-7×7 reconstructed surface by transmission electron diffraction', *Surf. Sci*., Vol. 164, p.367–392.

10 Uhrberg, R.I.G. and Hansson, G.V. (1991) 'Electronic structure of silicon surfaces: clean and with ordered overlayers', *Crit. Rev. Solid State Mater. Sci.*, Vol. 17, No. 2, p.133–186.

11 Venables, J.A. (2000) *Introduction to Surface and Thin Film Processes*, Cambridge University Press, Cambridge, England.

12 Lander, J.J. and Morrison, J. (1965) 'Surface reactions of silicon (111) with Aluminum and Indium', *J. Appl. Phys*., Vol. 36, No. 5, p.1706–1713.

13 Gallus, O., Pillo, Th., Hengsberger, M., Segovia, P. and Baer, Y. (2001) 'A system with a complex phase transition: Indium chains on Si(111)', *Euro. Phys. J. B*, Vol. 20, No. 3, p.313–319.

14 Nogami, J., Park, S. and Quate, C.F. (1987) 'Indium-induced reconstructions of the Si(111) surface studied by scanning tunneling microscopy', *Phys. Rev. B*, Vol. 36, No. 11, p.6221–6224.

15 Park, S., Nogami, J. and Quate, C.F. (1988) 'Metal-induced reconstructions of the silicon(111) surface', *J. Microsc.*, Vol. 152, No. 3, p.727–734.

16 OMahony, J.D., Patterson, C.H., McGilp, J.F., Leibsle, F.M., Weightman, P. and Flipse, C.F.J. (1992) 'The Au-induced 5×2 reconstruction on Si(111)', *Surf. Sci. Lett*., Vol. 277, Nos. 1–2, p.L57–L62.

17 Erwin, S.C. and Weitering, H.H. (1998) 'Theory of the 'Honeycomb Chain-Channel' reconstruction on M/Si(111)-(3×1)', *Phys. Rev. Lett*., Vol. 81, No. 11, p.2296–2299.

18 Carpinelli, J.M. (1995) 'Scanning tunneling microscopy study of the metal-induced Si(111)3×1 reconstruction: evidence for dimerized chain formation', *Surf. Sci*., Vol. 333 (Part B), p.1015–1021.

19 Weitering, H.H., Shi, X. and Erwin, S.C. (1996) 'Band dispersion of the ´ bonded-chain reconstruction of Si(111)3×1-Li: a critical evaluation of theory and experiment', *Phys. Rev. B*, Vol. 54, No. 15, p.10585–10592.

20 Stevens, J.L., Worthington, M.S. and Tsong, I.S.T. (1993) '4×1 reconstruction of indium deposited on vicinal Si(111) surfaces', *Phys. Rev. B*, Vol. 47, No. 3, p.1453–1459.

21 Abukawa, T., Sasaki, M., Hisamatsu, F., Goto, T., Kinoshita, T., Kakizaki, A. and Kono, S. (1995) 'Surface electronic structure of a single-domain Si(111)4×1-In surface: a synchrotron radiation photoemission study', *Surf. Sci*., Vol. 325, No. 2, p.33.

22 Himpsel, F.J. and Ortega, J.E. (1994) 'Edge state and terrace state for Cu on W(331) and W(110)', *Phys. Rev. B*, Vol. 50, No. 7, p.4992–4995.

23 Lipton-Duffin, J., MacLeod, J.M. and McLean, A.B. (2006) 'Detection of a Fermi level crossing in Si(557)-Au with inverse photoemission', *Phys. Rev. B*, Vol. 73, p.245418.

24 Himpsel, F.J., McChesney, J.L., Crain, J.N., Kirakosian, A., Prez-Dieste, V., Abbot, N., Luk, L., Yan-Yeung Nealey, P.F. and Petrovykh, D.Y. (2004) 'Stepped silicon surfaces as templates for one-dimensional nanostructures', *J. Phys. Chem. B*, Vol. 108, p.14484–14490.

25 Himpsel, F.J., Kirakosian, A., Crain, J.N., Lin, J.L. and Petrovykh, D.Y. (2001) 'Self-assembly of one-dimensional nanostructures at silicon surfaces', *Solid State Commun*., Vol. 117, p.149–157.

26 Himpsel, F.J., Altmann, K.N., Bennewitz, R., Crain, J.N., Kirakosian, A., Lin, J.L. and McChesney, J.L. (2001) 'One-dimensional electronic states at surfaces', *J. Phys.: Condens. Matter*, Vol. 13, p.11097–11113.

27 Segovia, P., Purdie, D., Hengsberger, M. and Baer, Y. (1999) 'Observation of spin and charge collective modes in one-dimensional metallic chains', *Nature*, Vol. 402, p.504–507.

28 Wilson, J.A., Di Salvo, F.J. and Mahajan, S. (1974) 'Charge-density waves in metallic, layered, transition-metal dichalcogenides', *Phys. Rev. Lett*., Vol. 32, p.8820885.

29 Thorne, R.E. (1996) 'Charge-density-wave conductors', *Phys. Today*, p.41–47.

30 Tossatti, E. (1995) *Electronic Surface and Interface States on Metallic Systems, in Surface States, Surface Metal-Insulator and Surface Insulator-Metal Transitions*, World Scientific, Singapore.

31 Dowben, P.A. (2000) 'The metallicity of thin films and overlayers', *Surf. Sci. Rep*., Vol. 40, p.151–247.

32 Tetsuyu, A. (2002) 'Charge-density waves on metal surfaces', *J. Phys.: Condens. Matter*, Vol. 14, p.8393–8414.

33 Haldane, F.D.M. (1981) 'Luttinger liquid theory of one-dimensional quantum fluids. 1. Properties of the Luttinger model and their extension to the general 1D interacting spinless Fermi gas', *J. Phys. C*, Vol. 14, No. 19, p.2585–2609.

34 Voit, J. (1993) 'Charge-spin separation and the spectral properties of Luttinger liquids', *Phys. Rev. B*, Vol. 46, No. 11, p.6740–6743.

35 Luttinger, J.M. (1963) 'An exactly soluble model of a many-fermion system', *J. Math. Phys*., Vol. 4, p.1154–1162.

36 DiNardo, N.J. (1994) *Nanoscale Characterization of Surface and Interfaces*, VCH, p.173.

37 Brihuega, I., Custance, O.P. and Rubén Gmez-Reodrguez, J.M. (2005) 'Instrinsic character of the (3×3) to (ã3×ã3) phase transition in Pb/Si(111)', *Phys. Rev. Lett*., Vol. 94, p.046101.

38 Lucas, A. (2000) *Design and Commissioning of a UHV-STM: Simplified Besocke Design for the Study of Nanowires*, University of Stuttgart, Stuttgart.

39 MacLeod, J.M., Moffat, Antje Miwa, J.A., Mark, A.G., Mullins, G.K., Dumont, R.H.J., Constant, G.E. and McLean, A.B. (2003) 'Two linear beetle-type scanning tunneling microscopes', *Rev. Sci. Instrum*., Vol. 74, No. 4, p.2429–2437.

40 MacLeod, J.M. (2006) 'Scanning tunneling microscopy characterization of nanoscale structures grown on low-index silicon surfaces', *Physics*, Queens University, Kingston, p.169.

41 Stoffel, N.G. and Johnson, P.D. (1984) 'A low-energy high-brightness electron gun for inverse photoemission', *Nucl. Instrum. Methods*, Vol. A234, p.230–234.

42 Lipton-Duffin, J. (2001) 'First results from a third generation KRIPES system', *Physics*, Queen's University, Kingston, p.75.

43 Lipton-Duffin, J.A., Mark, A.G. and McLean, A.B. (2002) 'Photon detection with n-propanol and C_2H_6O isomers', *Rev. Sci. Instrum*., Vol. 73, No. 9, p.3149–3153.

44 Lipton-Duffin, J.A., Mark, A.G., Mullins, G.K., Contant, G.E. and McLean, A.B. (2004) 'An inverse photoemission system with large solid angle of detection and adjustable optical bandpass', *Rev. Sci. Instrum*., Vol. 75, No. 2, p.445–454.

45 Hill, I.G. and McLean, A.B. (2000) 'Inverse photoemission studies of two quasi-one-dimensional overlayer systems', *Appl. Surf. Sci.*, Vols. 123–124, p.371–375.

46 Hill, I.G. and McLean, A.B. (1999) 'Detection of a Fermi level crossing in three-domain Si(111)-In(4×1)', *Phys. Rev. B*, Vol. 59, No. 15, p.9791–9793.

47 Hill, I.G. and McLean, A.B. (1999) 'Strongly anisotropic band dispersion of an image state located above metallic nanowires', *Phys. Rev. Lett*., Vol. 82, No. 10, p.2155–2158.

48 Hill, I.G. and McLean, A.B. (1998) 'Inverse photoemission studies of two quasi-one-dimensional overlayer systems', *Appl. Surf. Sci*., Vols. 123–124, p.371–375.

49 Hill, I.G. and McLean, A.B. (1997) 'Metallicity of In chains on Si(111)', *Phys. Rev. B*, Vol. 56, No. 24, p.15725–15728.

50 Bunk, O., Falkenberg, G., Zeysing, J.H., Lottermoser, L. and Johnson, R.L. (1999) 'Structure determination of the indium-induced Si(111)-(4×1) reconstruction by surface x-ray diffraction', *Phys. Rev. B*, Vol. 59, No. 19, p.12228–12231.

51 Lee, G., Yu, S.Y., Kim, H., Koo, J.Y., Lee, H. and Moon, D.W. (2003) 'Absolute in coverage and bias-dependent STM images of the Si(111)4×1-In surface', *Phys. Rev. B*, Vol. 67, p.035327.

52 McLean, A.B. and Hill, I.G. (2000) 'Probing the internal structure of nanowires', *Appl. Surf. Sci*., Vols. 162–163, p.620–624.

53 Yeom, H.W., Takeda, S., Rotenberg, E., Matsuda, I., Horikoshi, K., Lee, C.M., Kevan, S.D., Ohta, T., Nagao, T. and Hasegawa, S. (1999) 'Instability and charge density wave of metallic quantum chains on a silicon surface', *Phys. Rev. Lett*., Vol. 82, No. 24, p.4898–4901.

54 Kumpf, C., Bunk, O., Su, Y., Nielsen, M., Johnson, R.L., Fiedenhans'l, R. and Bechgaard, K. (2000) 'Low-temperature structure of indium quantum chains on silicon', *Phys. Rev. Lett*., Vol. 85, No. 23, p.4916.

55 Peierls, R.E. (1964) *Quantum Theory of Solids*, Clarendon, Oxford.

56 Gruner, G. (1994) *Density Waves in Solids*, Addison-Wesley, Reading, MA.

57 Sakamoto, K., Kyoya, K., Miki, K. and Matsuhata, H. (2000) 'Angle-resolved high-resolution electron-energy-loss study of In-adsorbed Si(111)-4×1 and -(8×2) surfaces', *Phys. Rev. B*, Vol. 62, No. 15, p.9923.

58 Cho, J.H. *et al*. (2001) 'Weakly correlated one-dimensional indium chains on Si(111)', *Phys. Rev. B*, Vol. 64, p.235302.

59 González, C., Flores, F. and Ortega, J. (2006) 'Soft phonon, dynamical fluctuations, and a reversible phase transition: indium chains on silicon', *Phys. Rev. Lett*., Vol. 96, p.136101.

60 Miwa, R.H. and Srivastava, G.P. (2001) 'Atomic geometry, electronic structure and image state for Si(111)-In(4×1)', *Surf. Sci*., Vol. 473, p.123–132.

61 Lee, G., Guo, J. and Plummer, E.W. (2005) 'Real-space observations of nanoscale inhomogeneities and fluctuations in a phase transition of a surface quasi-one-dimensional system: In/Si(111)', *Phys. Rev. Lett*., Vol. 95, p.116103.

62 Lee, G., Yu, S.Y., Kim, H. and Koo, J.Y. (2004) 'Defect-induced perturbation on Si(111)4×1-In: period-doubling modulations and its origin', *Phys. Rev. B*, Vol. 70, p.121304(R).

63 Guo, J., Lee, C. and Plummer, E.W. (2005) 'Intertwined electronic and structural phase transitions in the In/Si(111) interface', *Phys. Rev. Lett*., Vol. 95, p.046102.

64 Öfner, H., Surnev, S.L., Shapira, Y. and Netzer, F.P. (1994) 'Spectroscopy of interface states of indium-Si(111)(4×1) and (1×1)R30 surfaces', *Surf. Sci*., Vols. 307–309, p.315–320.

65 Nakamura, J., Watanabe, S. and Aono, M. (2001) 'Anisotropic electronic structure of the Si(111)-(4×1)In surface', *Phys. Rev. B*, Vol. 63, p.193307.

66 Srivastava, G.P. (1999) *Theoretical Modelling of Semiconductor Surfaces*, World Scientific, Singapore.

67 Osgood Jr., R.M. and Wang, X. (1998) 'Image states on single-crystal metal surface', in Ehrenreich, H. and Spaepen, F. (Eds.): *Solid State Physics; Image States on Single-Crystal Metal Surface*, New York, Academic, Vol. 51, pp.1–80.

68 Crain, J.N., Kirakosian, A., Altmann, K.N., Bromberger, C., Erwin, S.G., McChesney, J.L., Lin, J.L. and Himpsel, F.J. (2003) 'Fractional band filling in an atomic chain structure', *Phys. Rev. Lett*., Vol. 90, p.176805.

69 Crain, J.N., McChesney, J.L., Zheng, F., Gallagher, M.C., Snijders, P.C., Bissen, M., Gundelach, C., Erwin, S.G. and Himpsel, F.J. (2004) 'Electronic structure of atomic chains on vicinal Si(111)-Au', *Phys. Rev. B*, Vol. 69, p.125401.

70 Robinson, I.K., Bennett, P.A. and Himpsel, F.J. (2002) 'Structure of quantum wires in Au/Si(557)', *Phys. Rev. Lett*., Vol. 88, No. 9, p.096104.

71 Kirakosian, A., Bennewitz, R., Crain, J.N., Fauster, T., Lin, J.L., Petrovykh, D.Y. and Himpsel, F.J. (2001) 'Atomically accurate Si grating with 5.73 period', *Appl. Phys. Lett*., Vol. 79, No. 11, p.1608–1610.

72 Crain, J.N. and Himpsel, F.J. (2006) 'Low-dimensional electronic states at silicon surfaces', *Appl. Phys. A*, Vol. 82, p.431–438.

73 McChesney, J.L., Crain, J.N., Pérez-Dieste, V., Fan Zheng, Gallagher, M.C., Bissen, M., Gundelach, C. and Himpsel, F.J. (2004) 'Electronic stabilization of a 5×4 dopant superlattice on Si(111)5×2-Au', *Phys. Rev. B*, Vol. 70, p.195430.

74 Bertel, E. (1995) 'One- and two-dimensional surface states on metals', *Surf. Sci*., Vols. 331–333, p.1136–1146.

75 Ahn, J.R., Yeom, H.W., Yoon, H.S. and Lyo, I.W. (2003) 'Metal-insulator transition in Au atomic chains on Si with two proximal bands', *Phys. Rev. Lett*., Vol. 91, p.196403.

76 Portal, D.S., Riikonen, S. and Martin, R.M. (2004) 'Role of spin-orbit splitting and dynamical fluctuations in the Si(557)-Au surface', *Phys. Rev. Lett*., Vol. 93, p.146803.

77 Losio, R., Altmann, K.N., Kirakosian, A., Lin, J.L., Petrovykh, D.Y. and Himpsel, F.J. (2001) 'Band splitting for Si(557)-Au: Is it spin-charge separation?', *Phys. Rev. Lett*., Vol. 86, p.4632–4635.

78 LaShell, S., McDougall, B.A. and Jensen, E. (1996) 'Spin splitting of Au(111) surface state band observed with angle resolved photoelectron spectroscopy', *Phys. Rev. Lett*., Vol. 77, No. 16, p.3419–3422.

79 Altmann, K.N., Crain, J.N., Kirakosian, A., Lin, J.L., Petrovykh, D.Y. and Himpsel, F.J. (2001) 'Electronic structure of atomic chains on vicinal Si(111)-Au', *Phys. Rev. B*, Vol. 64, p.035406.

80 Osgood Jr., R.M. and Wang, X. (1998) 'Image states on single-crystal metal surface', *Solid State Phys.*, Vol. 51, p.1–80.

81 Heskett, D., Frank, K-H., Koch, E.E. and Freund, H.J. (1987) 'Unoccupied electron band structure of Na overlayers on Al(111)', *Phys. Rev. B*, Vol. 36, p.R1276–R1279.

82 Yang, S., Bartynski, R.A. and Vanderbilt, D. (1994) 'Unoccupied electronic structure of Al(111)', *Phys. Rev. B*, Vol. 50, p.12025–12032.

83 Chulkov, E.V., Silkin, V.M. and Echenique, P.M. (1999) 'Image potential states on metal surfaces: binding energies and wave functions', *Surf. Sci*., Vol. 437, p.330–352.

84 Lindgren, S.Ä. and Walldém, L. (1989) 'Resonant bounds states for simple metal surfaces', *Phys. Rev. B*, Vol. 40, No. 17, p.11546–11548.

85 Salmi, L-A. and Persson, M. (1989) 'Electron resonances in alkali-metal overlayers on metals', *Phys. Rev. B*, Vol. 39, No. 9, p.6249–6252.

86 Fauster, T. (1994) 'Two-photon photoemission', *Prog. Surf. Sci*., Vol. 46, p.177.

87 Fauster, T. (1995) 'Growth and morphology of ultrathin metal films studied by the high-resolution spectroscopy of image states through two-photon photoemission', in Bertel, E. and Donath, M. (Eds.): *Electronic Surface and Interface States on Metallic Systems*, World Scientific, Singapore, pp.171–186.

88 Fauster, Th., Reuss, Ch., Shumay, I.L. and Weinelt, M. (2000) 'Femtosecond two-photon photoemission studies of image-potential states', *Chem. Phys*., Vol. 251, p.111.

89 Naitoh, M., Shimaya, H., Nishigaki, S., Oishi, N. and Shoji, F. (1997) 'Scanning tunneling microscopy observation of bismuth growth on Si(100) surfaces', *Surf. Sci*., Vols. 377–379, p.899–903.

90 Owen, J.H.G., Miki, K. and Bowler, D.R. (2006) 'Self-assembled nanowires on semiconductor surfaces', *J. Mater. Sci*., Vol. 41, No. 14, July, pp.4568–4603.

91 Naitoh, M., Shimiya, H., Nishigaki, S., Oishi, N. and Shoji, F. (1999) 'Bismuth-induced surface structure of Si(100) studied by scanning tunneling microscopy', *Appl. Surf. Sci*., Vol. 142, p.38–42.

92 Naitoh, M., Takei, M., Nishigaki, S., Oishi, N. and Shoji, F. (2001) 'Scanning tunneling microscopy observation of Bi-induced surface structures on the Si(100) surface', *Surf. Sci*., Vols. 482–485, p.1440–1444.

93 Naitoh, M., Takei, M., Nishigaki, S., Oishi, N. and Shoji, F. (2000) 'Structure of Bi-dimer linear chains on a Si(100) surface: a scanning tunneling microscopy study', *Jpn. J. Appl. Phys*., Vol. 39, p.2793, 2794.

94 Bowler, D.R. and Owen, J.H.G. (2002) 'Structure of Bi nanolines: using tight binding to search parameter space', *J. Phys.: Condens. Matter*, Vol. 14, p.6761–6769.

95 Miki, K., Bowler, D.R., Owen, J.H.G., Briggs, G.A.D. and Sakamoto, K. (1999) 'Atomically perfect bismuth lines on Si(001)', *Phys. Rev. B*, Vol. 59, No. 23, p.14868–14871.

96 Miki, K., Matsuhata, H., Sakamoto, K., Briggs, G.A.D., Owen, J.H.G. and Bowler, D.R. (1999) 'Bismuth and antimony nanolines in a Si epitaxial layer', *Proceedings, Institute of Physics Conf. Series*, Vol. 164, p.167–170.

97 Owen, J.H.G., Bowler, D.R. and Miki, K. (2002) 'Bi nanoline passivity to attack by radical hydrogen or oxygen', *Surf. Sci*., Vol. 499, p.L124–L128.

98 Owen, J.H.G., Bowler, D.R. and Miki, K. (2005) 'Identification of intermediate linear structure formed during Bi/Si(001) surface anneal', *Surf. Sci*., Vol. 596, No. 103, p.163–175.

99 Owen, J.H.G., Miki, K. and Bowler, D.R. (2003) 'Interaction between electronic structure and strain in Bi nanolines on Si(001)', *Surf. Sci. Lett*., Vol. 527, p.L177–L183.

100 Owen, J.H.G. *et al*. (2002) 'Stress relief as the driving force for self-assembled Bi nanolines', *Phys. Rev. Lett*., Vol. 88, p.226104.

101 MacLeod, J.M. and McLean, A.B. (2004) 'Single 2×1 domain orientation on Si(001) surfaces using a periodic Bi line arrays', *Phys. Rev. B*, Vol. 70, p.041306(R).

102 Lopinski, G.P., Wayner, D.D.M. and Wolkow, R.A. (2000) 'Self-directed growth of molecular nanostructures on silicon', *Nature*, Vol. 406, p.48–51.

103 Hossain, M.Z., Kato, H.S. and Kawai, M. (2005) 'Controlled fabrication of 1D molecular lines across the dimer rows on the Si(100)-(2×1) surface through the radical chain reaction', *J. Am. Chem. Soc*., Vol. 127, p.15030–15031.

104 Hossain, M.Z., Kato, H.S. and Kawai, M. (2005) 'Fabrication of interconnected 1D molecular lines along and across the dimer rows on the Si(100)-(2×1)-H surface through the radical chain reaction', *J. Phys. Chem. Lett. B*, Vol. 109, p.23129.

105 Hecht, S. (2003) 'Welding, organizing, and planting organic molecules on substrate surface – promising approaches towards nanoarchitectonics from the bottom up', *Angew. Chem., Int. Ed*., Vol. 42, No. 1, p.24, 25.

106 Miwa, R.H., Schmidt, T.M. and Srivastava, G.P. (2002) 'Ab initio study of self-organized Bi lines on the Si(001) surface', *Surf. Sci*., Vols. 507–510, p.368–373.

107 Miwa, R.H. and Srivastava, G.P. (2002) 'Self-organized Bi lines on the Si(001) surface: a theoretical study', *Phys. Rev. B*, Vol. 66, No. 12, p.235317.

108 Marrian, C.R.K. and Tennant, D.M. (2003) 'Nanofabrication', *J. Vac. Sci. Technol*., Vol. A21, p.S207–S215.

109 de Feyter, S. and de Schryver, F.C. (2003) 'Two-dimensional supramolecular self-assembly probed by scanning tunneling microscopy', *Chem. Soc. Rev*., Vol. 32, p.139–150.

110 Zhang, Z. and Lagally, M.G. (1997) 'Atomistic processes in the early stages of thin-film growth', *Science*, Vol. 276, p.377–383.

111 Steinfort, A.J., Scholte, P.M.L.O., Ettema, A., Tuinstra, F., Nielsen, M., Landemark E., Smilgies, D-M., Feidenhans'l, R., Falkenberg, G., Seehofer, L. and Johnson, R.L. (1996) 'Strain in nanoscale germanium hut clusters on Si(001) studied by x-ray diffraction', *Phys. Rev. Lett*., Vol. 77, No. 10, p.2009–2012.

112 Motta, N., Sgarlata, A., Calarco, R., Nguyen, Q., Prosposito, P., Balzarotti, A. and de Crescenzi, M. (1998) 'Scanning tunneling microscopy studies of Ge/Si films on Si(111): from layer by layer to quantum dots', *J. Vac. Sci. Technol*., Vol. B16, p.1555–1559.

113 Mo, Y.W., Savage, D.E., Swartzentruber, B.S. and Lagally, M.G. (1990) 'Kinetic pathways in stranski-krastanov growth on Ge on Si(001)', *Phys. Rev. Lett*., Vol. 65, p.1020.

114 Eaglesham, D.J. and Cerullo, M. (1990) 'Dislocation-free stranski-krastanow growth of Ge on Si(100)', *Phys. Rev. Lett*., Vol. 64, p.1943–1946.

115 Chen, Y., Ohlberg, D.A.A., Medeiros-Ribeiro, G., Chang, Y.A. and Williams, R.S. (2000) 'Stabilities of single-layer and bilayer steps on Si(001) surfaces', *Appl. Phys. Lett*., Vol. 76, p.4004–4006.

116 Liu, B.Z. and Nogami, J. (2003) 'Growth of parallel rare-earth silicide nanowire arrays on vicinal Si(001)', *Nanotechnol*ogy, Vol. 14, p.873–877.

117 Tersoff, J. and Hamann, D.R. (1985) 'Theory of the scanning tunneling microscope', *Phys. Rev. B*, Vol. 31, p.805–813.

118 Miwa, R.H., MacLeod, J.M. McLean, A.B. and Srivastava, G.P. (2005) 'The equilibrium geometry and electronic structure of Bi nanolines on clean and hydrogenated Si(001) surfaces', *Nanotechnol*ogy, Vol. 16, p.2427–2435.

119 Ceperley, D.M. and Alder, B.J. (1980) 'Ground state of the electron gas by a stochastic method', *Phys. Rev. Lett*., Vol. 45, p.566–569.

120 Perdew, J.P. and Zunger, A. (1981) 'Self-interaction correction to density-functional approximations for many-electron systems', *Phys. Rev. B*, Vol. 23, p.5048–5079.

121 Kleinman, L. and Bylander, D.M. (1982) 'Efficacious form for model pseudopotentials', *Phys. Rev. Lett*., Vol. 48, p.1425.

122 Gonze, X., Stumpf, R. and Scheffler, M. (1991) 'Analysis of separable potentials', *Phys. Rev. B*, Vol. 44, p.8503–8513.

123 Neugebauer, J. and Scheffler, M. (1992) 'Adsorbate-substrate and adsorbate-adsorbate interactions of Na and K adlayers on Al(111)', *Phys. Rev. B*, Vol. 46, No. 24, p.16067.

124 Bengtsson, L. (1999) 'Dipole correction for surface supercell calculations', *Phys. Rev. B*, Vol. 59, p.12301–12304.

125 Tersoff, J. and Hamann, D.R. (1983) 'Theory and application for the scanning tunneling microscope', *Phys. Rev. Lett*., Vol. 50, p.1998–2001.

126 Miwa, R.H., MacLeod, J.M., Srivastava, G.P. and McLean, A.B. (2005) 'The geometry of Bi nanolines on Si(001)', *Appl. Surf. Sci*., Vol. 244, Nos. 1–4, p.157–160.

127 He, Y. and Che, J.G. (2004) 'Stress relief from missing dimers on BiSi(001)', *Surf. Sci*., Vol. 569, p.176–184.

128 Mark, A.G., Lipton-Duffin, J.A., MacLeod, J.M., Miwa, R.H., Srivastava, G.P. and McLean, A.B. (2005) 'The electronic structure of Si(001)-Bi(2×n)', *J. Phys.: Condens. Matter*, Vol. 17, No. 4, p.571–580.

129 Park, C., Bakhtizin, R.Z., Hashizume, T. and Sakurai, T. (1994) 'Strain relief and ordering of (2×n)-Bi structure on Si(100)', *J. Vac. Sci. Technol*., Vol. B32, No. 3, p.2049–2051.

130 Alerhand, O.L., Vanderbilt, D., Meade, R.D. and Joannopoulos, J.D. (1988) 'Spontaneous formation of stress domain on crystal surfaces', *Phys. Rev. Lett*., Vol. 61, No. 17, p.1973–1976.

131 Kubo, O., Ryu, J.T., Tani, H., Harada, T., Kobayashi, T., Katayama, M. and Oura, K. (2001) 'STM study of structural changes on Si(100)2×1-Sb surface induced by atomic hydrogen', *Appl. Surf. Sci*., Vols. 169–170, p.93–99.

132 Wang, J.T., Mizuseki, H., Kawazow, Y., Hashizume, T., Naitoh, M., Wang, D.S. and Wang, E.G. (2003) 'Stability of Sb line structures on Si(001)', *Phys. Rev. B*, Vol. 67, p.193307.

133 Wang, Jian-Tao Wang, E.G., Wang, D.S., Mizuseki, H., Kawazoe, Y., Naitoh, M. and Nishigaki, S. (2005) 'Dynamic ad-dimer twisting assisted nanowire self-assembly on Si(001)', *Phys. Rev. Lett*., Vol. 94, p.226103.

134 MacLeod, J.M., Miwa, R.H., Srivastava, G.P. and McLean, A.B. (2005) 'The electronic origin of contrast reversal in bias-dependent STM images of nanolines', *Surf. Sci.*, Vol. 576, Nos. 1–3, p.116–122.

135 Zhang, S.B., McMahon, W.E., Olson, J.M. and Wei, S.H. (2001) 'Steps on As-terminated Ge(001) revisited: theory versus experiment', *Phys. Rev. Lett*., Vol. 87, No. 16, p.166104.

136 McMahon, W.E., Batyrev, I., Hannappel, T., Olson, J.M. and Zhang, H.M. (2006) '5-7-5 line defects on As/Si(100): a general stress-relief mechanism for V/iV surfaces', *Phys. Rev. B*, Vol. 74, p.033304.